

CHALMERS



BRAKE BY WIRE SYSTEM FOR CONSTRUCTION VEHICLES

MODEL BASED CONTROLLER DESIGN AND
PROOF-OF-CONCEPT TESTING

KARL STJÄRNE
PATRIK WERNER

Master Thesis
Department of Signals and Systems
CHALMERS UNIVERSITY OF TECHNOLOGY
Göteborg, Sweden

EX29/2014

BRAKE BY WIRE SYSTEM FOR CONSTRUCTION VEHICLES - MODEL
BASED CONTROLLER DESIGN AND PROOF-OF-CONCEPT TESTING

KARL STJÄRNE, PATRIK WERNER

© KARL STJÄRNE, PATRIK WERNER, 2014

Master's Thesis EX29/2014
Departments of Signals and Systems
Chalmers University of Technology
SE-412 96 Göteborg
Sweden
Telephone: + 46 (0)31-772 1000

Cover:
Volvo L220F wheel loader. (Courtesy of Volvo CE, AB Volvo)

Departments of Signals and Systems
Göteborg, Sweden 2014

Abstract

This thesis investigates and proposes a brake-by-wire system for wheel based construction vehicles. The brake-by-wire system consists of an actuator controller that controls the brake valve, a manually controlled electrical brake pedal and a closed-loop retardation controller. The brake-by-wire system was proof of concept tested on a Volvo L220F wheel loader.

In addition to this, an anti-lock brake system is proposed together with an extended Kalman filter that estimates the vehicle velocity, wheel slip and surface friction coefficient based on wheel speed and acceleration. From simulations it was shown that wheel lock is not very probable except in poor surface conditions.

A brief risk analysis and safety assessment was conducted on the brake system according to ISO-26262 to identify the possible hazardous event that the brake system might cause.

During the proof of concept test it was shown that the system indeed is working, even though more evaluation and tuning is needed to improve performance.

KEYWORDS: Brake by Wire, Anti-lock Brake System, ABS, Retardation control, Extended Kalman Filter

Preface

This Master's Thesis was carried out at CPAC Systems AB located in Gothenburg, Sweden, during the spring semester of 2014. CPAC Systems AB is a part of the Volvo Group.

Acknowledgments

The authors would like to give a special thank to their supervisor at CPAC Marcus Broberg for his support throughout the project, Michael Årnevall for his help with the vehicle testing, Oscar Leon for his support regarding hardware issues and last but not least all the numerous people at CPAC Systems who has help us with various things.

Göteborg, September 29, 2014

KARL STJÄRNE, PATRIK WERNER

Notations

Abbreviations

ABS	Anti-lock Braking System
AIS	Abbreviated Injury Scale
ASIL	Automotive Safety Integrity Level
BbW	Brake by Wire
CAN	Controlled Area Network
DOF	Degrees Of Freedom
ECU	Electronic Control Unit
FMEA	Failure Mode and Effect Analysis
FSR	Functional Safety Requirement
FTA	Fault Tree Analysis
IEC	International Electrotechnical Commission
IMU	Inertial Measurement Unit
ISO	International Standard Organization
LHP	Left Half Plane
NA	Not Available
PI	Proportional-Integral
PID	Proportional-Integral-Derivative
PWM	Pulse Width Modulation
RHP	Right Half Plane
RMS	Root Mean Square
SG	Safety Goal
VRU	Vulnerable Road Users

Capital Letters

A	System matrix, Amplitude
B	Input matrix
C	Output matrix, Controllability
E	Exposure
F	Force [N]
I	Current [A], Identity matrix
J	Inertia
K	Gain
M	Maximum
Q	Covariance matrix
R	Covariance matrix
S	Sensitivity function, Severity
T	Torque [Nm], Complementary sensitivity function
V	Voltage [V]

Small Letters

a	Numerical constant, Acceleration
b	Numerical constant
c	Numerical constant
e	Error,
g	Gravitational constant
h	Hysteresis, Height [m], Sample time
k	Gain
l	Length [m]
m	Mass [kg]
p	Pole
r	Radius
s	Operator variable in the Laplace domain
t	Time [s]
u	Control signal
v	Vehicle velocity [m/s]
z	Zero

Greek Letters

α	Numerical constant
β	Numerical constant
λ	Normalized wheel slip
μ	Friction coefficient
ω	Wheel rotational velocity [rad/s]
φ	Phase
τ	Time constant
ζ	Damping ratio

Subscripts

0	Equilibrium, initial
<i>act</i>	Actual
<i>b</i>	Brake
<i>c</i>	Crossover
<i>crit</i>	Critical
<i>d</i>	Derivative
<i>err</i>	Error
<i>f</i>	Front
<i>i</i>	Integral
<i>in</i>	Input
<i>k</i>	Discrete time index
<i>m</i>	Margin
<i>n</i>	Natural
<i>on</i>	Enabled
<i>out</i>	Output
<i>p</i>	Proportional
<i>r</i>	Rear
<i>req</i>	Requested
<i>sp</i>	Setpoint
<i>thresh</i>	Threshold
<i>v</i>	Velocity
<i>x</i>	X-direction
<i>z</i>	Z-direction

Superscripts

<i>T</i>	Transpose
----------	-----------

Diacritical marks

$\hat{}$	Approximation or estimate
$\bar{}$	Mean or average
$\tilde{}$	Residual
$\dot{}$	Time derivative

Contents

1	Introduction	1
1.1	Scope	1
1.2	Problem definition	2
1.3	Method and Limitations	2
1.3.1	Modeling	3
1.3.2	Controller Synthesis	3
1.3.3	Risk Analysis and Safety Assessment	3
1.4	Report Outline	3
2	System Overview	5
2.1	Peripheral Devices	5
2.1.1	Driveline Control	5
2.1.2	Brake Pedal	6
2.1.3	Brake Actuator	6
2.1.4	Inertial Measurement Unit (IMU)	6
2.2	Brake System	6
2.2.1	Actuator Controller	6
2.2.2	Brake Controller	7
2.2.3	Observer	7
3	Modeling	8
3.1	Introduction	8
3.2	Single corner vehicle model	9
3.2.1	Linearization and Equilibrium points	10
3.3	Dual corner vehicle model	11

3.4	Anti Lock system	13
3.5	Wheel slip model	14
3.6	Brake actuator	14
4	Controller Design	16
4.1	Actuator Controller	17
4.2	Brake Pedal Controller	17
4.3	Retardation Controller	18
4.4	Anti-lock system	22
4.4.1	Wheel Slip Control	22
4.4.2	Anti-lock System Activation and Deactivation	25
4.5	Anti-windup and bumpless switching between controllers	26
4.6	State Observer	27
4.6.1	Extended Kalman Filter	28
5	ISO-26262 Theory	31
5.1	ISO 26262	31
5.1.1	Item definition	32
5.1.2	Hazard analysis and Risk Assessment	32
5.1.3	Safety Goals	33
5.1.4	Functional Safety Concept	33
6	System Test and Results	34
6.1	Simulations	34
6.1.1	Vehicle model	34
6.1.2	Wheel Slip Analysis	35
6.1.3	Retardation Controller	36
6.1.4	Anti-lock system	36
6.1.5	State Observer	38

6.2	Bench Testing	39
6.2.1	Actuator Controller	39
6.2.2	Brake Pedal Controller	39
6.2.3	Retardation Controller	40
6.2.4	Entire System	40
6.3	Vehicle Testing	42
6.3.1	Current Step Test	42
6.3.2	Acceleration Step Test	44
6.3.3	Brake Pedal Functionality Test	46
6.4	Risk Analysis and Safety Assessment	47
6.4.1	Item Definition	47
6.4.2	Operational Situations	47
6.4.3	System Malfunctions	48
6.4.4	Hazard analysis and Risk Assessment	49
6.4.5	Functional Safety Concept	49
7	Discussion	50
7.1	Brake Pedal Controller	50
7.2	Retardation controller	50
7.3	Dithering	50
7.4	State estimator and Slip controller	51
7.5	Future Work	52
8	Conclusions	53
8.1	Brake system	53
8.2	Safety assessment	53
	APPENDIX	i

A Operational Situations and Corresponding Exposure	i
B Fault Tree Analysis	ii
C Kalman Filter Based on Jerk	iv
D Current Step Test of Real Vehicle	v

1 Introduction

The X-by-wire technology originates from the airplane industry where it was referred to as Fly-by-wire. With Fly-by-wire the hydraulic linkage between the input and the actuator was replaced by electrical wires, thereof the name by-wire.

It was quickly shown that computerized electrical control could increase the performance significantly, both in maneuverability and stability, compared to the traditional mechanical steering [1][2][3]. Since the introduction in airplanes during the 70's the industrial demand for X-by-wire systems has been steadily increasing [6].

For more than two decades the automotive industry has given the X-by-wire technology attention and development has been carried out to incorporate this technology in production cars. The X-by-wire technology introduces the possibility to have a higher precision in monitoring and in the overall system which has lead to a better fuel economy. Also advanced collision avoidance systems require the possibility to intervene the driver inputs and co-ordinate multiple subsystems such as brakes, steering etc [11]. This type of control is not possible in traditional mechanical systems which has been a strong incentive for the development of X-by-wire systems in the automotive industry. So far X-by-wire systems is relatively new in the heavy-duty construction vehicle industry.

All commercial vehicles are equipped with a brake pedal. The brake pedal is normally directly connected physically to the brake system where the operator, i.e. the driver, builds the brake pressure manually or with the help of a brake servo. In a brake-by-wire system the brake pressure and the brake pedal are physically decoupled. The traditional brake pedal is instead substituted with an electrical sensor, which could be anything from a joystick, a pedal, button etc. In fact the brake input does not have to be a real physical signal since the brake input is processed by a microprocessor.

Replacing mechanical links with wires does not only reduce the mechanical complexity but it does also take up less physical space in the engine compartment. With the use of electronic sensors, more knowledge of the system and its environment can be gathered. With the help of computers, information can be shared between different subsystems, which allows for more sophisticated control strategies to be implemented.

1.1 Scope

This thesis will investigate and propose an electronic braking sub-system aimed towards construction vehicles. The system shall handle both normal brake pedal functionality and closed-loop retardation control. A brief risk analysis and safety

assessment according to ISO-26262 will be carried out.

1.2 Problem definition

The thesis' scope can be divided into the following subtasks:

Risk analysis and safety assessment

The resulting brake by wire system shall be investigated to a detailed level when it comes to reliability and functional safety. Safety-critical system components shall be identified using widely accepted methods such as failure mode and effect analysis (FMEA) or fault tree analysis (FTA). A full analysis according to the normative ISO-26262, further described in Chapter 5, is considered out of scope, but the philosophy therein delineated shall be pursued.

Mathematical modeling

Mathematical models shall be derived for both a construction vehicle and the brake actuator. These models will allow for controller synthesis and system verification.

Actuator controller

A controller for the brake actuator shall be synthesized. The actuator controller shall be stable with good reference tracking and a fast response such that the dynamics of the actuator controller are negligible compared to the vehicle dynamics.

Brake system controller

A controller that can input brake requests from both the brake pedal and from overlying vehicle control systems shall be designed. The brake system shall perform at least as good as the existing braking system regarding response time and damping. The brake performance should also be adequate enough to replace the existing brake system. The retardation controller should have good reference tracking, stable dynamics and the transition between the controllers should be smooth. Also, the possibilities and benefits from having an anti-lock system will be evaluated.

1.3 Method and Limitations

A brief description of the methods used are found in this chapter. The brake system will be verified through simulations, bench testing and proof-of-concept testing on a vehicle. The focus for the brake-by-wire system will lie on functionality and performance and not driver experience. The system shall be designed such that its functions are intuitive, but no analysis or methods in the topic "Human and Machine interaction" will be used to specify any demands on the system. Also, focus will lie on brake performance, e.g smooth and precise braking whereas design features such as haptic feedback is considered to be out of scope.

1.3.1 Modeling

The mathematical models shall be based on either well known mechanical relations derived from free body diagrams or identified from step response analysis. To simplify, suspension dynamics will be neglected, and only straight line longitudinal movement will be considered. Parameters will be acquired from datasheets or approximated from component testing.

1.3.2 Controller Synthesis

Simplicity and robustness are key factors for the control system. The initial controller versions will be based on stability analysis. The following controller versions are synthesized through an iterative method, in each step the controllers are tested and fine tuned until desired results are met. Figure 1.1 illustrates the work flow.

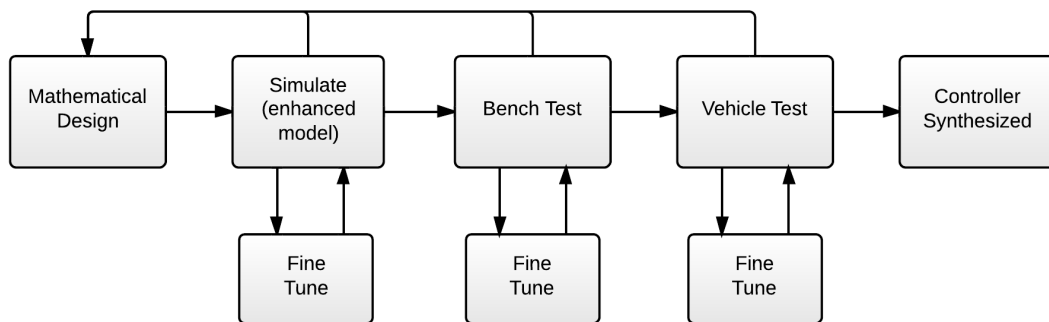


Figure 1.1. Controller synthesis work flow

1.3.3 Risk Analysis and Safety Assessment

Due to time restrictions a full ISO-26262 analysis will not be conducted. Chapter 5 further explains the ISO-26262 methodology.

1.4 Report Outline

First a general description of the system and its components are given in Chapter 2. Then the mathematical models that was used are presented together with some basic tire road friction properties in Chapter 3. In Chapter 4, the design approach of the different controllers are described. Chapter 5 gives a short introduction of the workflow of ISO-26262. Results from simulation and implementation of the controllers presented in Chapter 4 together with the ISO-26262 analysis are presented

in Chapter 6. The outcome of these results are then discussed in Chapter 7 and the conclusions drawn are given in Chapter 8.

2 System Overview

This chapter is intended to give the reader an overview of the brake-by-wire system, a conceptual schematics are presented in Figure 2.1. The system will process brake requests from both the overlaying driveline control system and the brake pedal. A torque request is calculated in the brake controller based on input brake requests and sensor measurements. The torque request is passed to and processed in an actuator controller, which controls the current through the actuator such that the braking torque is kept at a desired value.

Due to the fact that not all physical quantities are measurable and that some sensor data may be influenced by noise, an observer will be used for filtering and estimation.

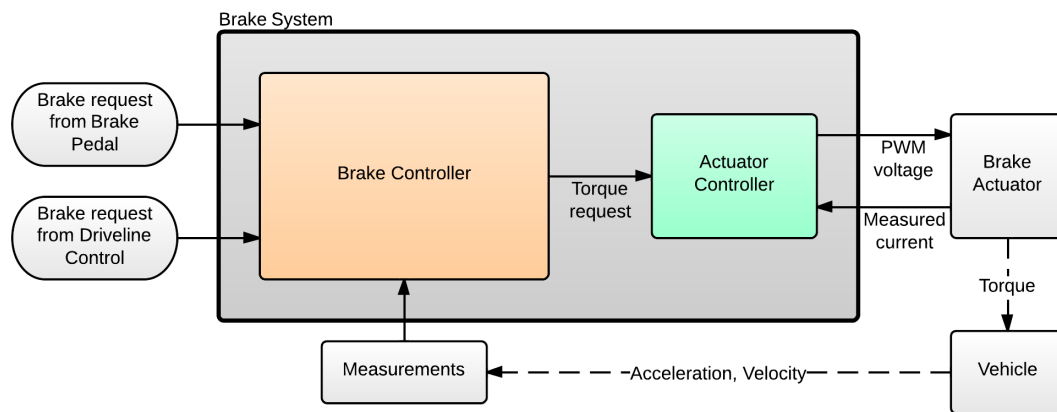


Figure 2.1. System overview

2.1 Peripheral Devices

The brake-by-wire system receives inputs from, and sends outputs to peripheral devices in the vehicle. These devices are listed in this chapter.

2.1.1 Driveline Control

The Driveline Control is an overlaying system which controls the entire vehicle driveline. It will issue brake requests in the form of a desired rate of acceleration.

2.1.2 Brake Pedal

This project will use an existing market pedal that generates an analogue voltage between 0.5 V and 4.5 V depending on the pedal angle.

2.1.3 Brake Actuator

The brake actuator serves as an interface between the electrical and the mechanical (hydraulic) part of the brake system. The actuator used in this project is a solenoid valve. The valve is electro mechanically operated and it is controlled by applying voltage to the solenoid winding and thereby pushing current through it. The current generates a force which pushes a plunger a certain distance. The valve is designed in such a way that a certain current through it will result in a certain output pressure.

2.1.4 Inertial Measurement Unit (IMU)

An IMU will provide measurements of the vehicle's acceleration to the retardation controller. The IMU will be an off the shelf 16-bit 3-DOF accelerometer with a measurable range of $\pm 2g$, with a error of approximately $\pm 3.5\%$ [10].

2.2 Brake System

The brake system, presented in Figure 2.1, will process the brake requests from the brake pedal and the driveline control together with the acceleration data from the IMU, the output from the system is a PWM voltage signal fed to the brake actuator. The brake system will be divided into several subsystems each serving a well defined purpose, each subsystem is described below.

2.2.1 Actuator Controller

The Actuator controller's task is to feed the brake actuator solenoid with the desired current. The primary design objectives for this controller are fast response time and low complexity, these objectives are based on the assumption that the electrical part of the brake system is much faster than the mechanical. The controller input is a torque reference and the controller output is a PWM voltage signal.

2.2.2 Brake Controller

The brake controller will process brake requests together with filtered sensor data from the observer. The brake controller will output a torque request which is sent to the actuator controller. The brake controller consists of the following subsystems:

Brake Pedal Controller

The Brake Pedal Controller's task is to map the actuation of the pedal to a desired braking torque, that is to emulate a traditional hydraulic brake pedal.

Retardation Controller

The retardation controller will process the retardation request from the Driveline control together with acceleration data from the observer. The controller calculates the necessary brake torque required to achieve and maintain the desired acceleration.

Anti-lock system

The anti-lock system will limit the input torque to the actuator controller so that the wheel slip does not exceed a near optimal degree. The anti-lock system inputs the requested torque, current degree of wheel slip and current vehicle velocity, the system's output is a torque request.

2.2.3 Observer

To allow for more sophisticated control architectures it is highly desired that many of the vehicle's parameters are available. However, many of the physical quantities, like vehicle velocity and wheel slip, are not measurable and therefore need to be estimated. The observer's task is to process data from both the brake controller and the measurement unit to not only estimate the non-measurable parameters, but also filter the measured data. To achieve this and due to the nonlinear properties of some of the quantities an extended Kalman filter was created as a observer. This filter is further explained in Chapter 4.6.

3 Modeling

3.1 Introduction

In order for a vehicle to decelerate, not considering any external braking force such as wind drag, its wheels has to have a lower tangential speed than the vehicle. This difference is often referred to as wheel slip and it is defined as:

$$\lambda(v, \omega) = \frac{v - \omega r}{v}, \lambda \in [0, 1] \tag{3.1}$$

where v is the velocity of the vehicle, ω is the rotational velocity of the wheel and r is the wheel radius.

When a brake torque is applied the wheel starts to decelerate, i.e the wheel slip increases which creates friction between the tire and the road. The friction depends on the amount of wheel slip and the surface. One famous model of the friction as a function of wheel slip is the Pacejka model, also known as the *magic formula*. This model has been shown to be able to match experimental measurements very accurately [9]. Figure 3.1 shows the friction coefficient, μ as a function of wheel slip, λ , according to this model for different road surfaces.

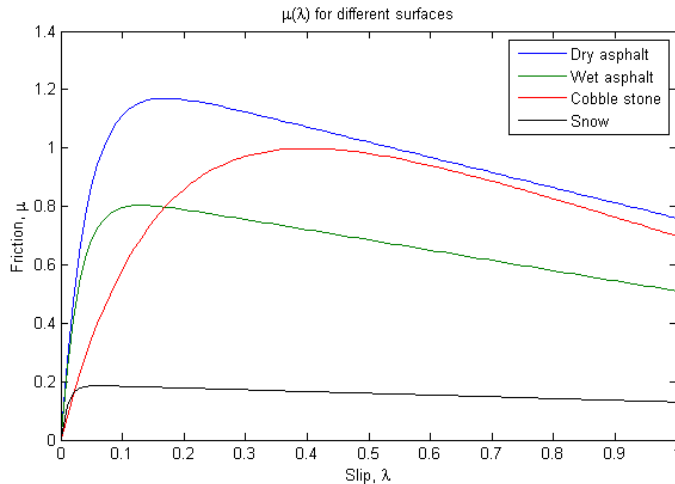


Figure 3.1. Friction, μ , as a function of wheel slip, λ

This shows that the friction, i.e effective brake force, heavily depends on the surface. The maximum friction between tire and road is roughly six times greater on dry asphalt compared to snow. Another thing to note is that every curve has a peak value with a decreasing slope to right of it. This means that beyond this peak less

brake torque is needed than previously to increase the wheel slip further. Intuitively, this kind of behavior indicates that the system is open-loop unstable to the right of the friction peak.

3.2 Single corner vehicle model

A simple approach towards a mathematical model for the vehicle dynamics is considering only one wheel and a sub part of the total vehicle mass. From the free body diagram in Figure 3.2 the following set of equations can be derived.

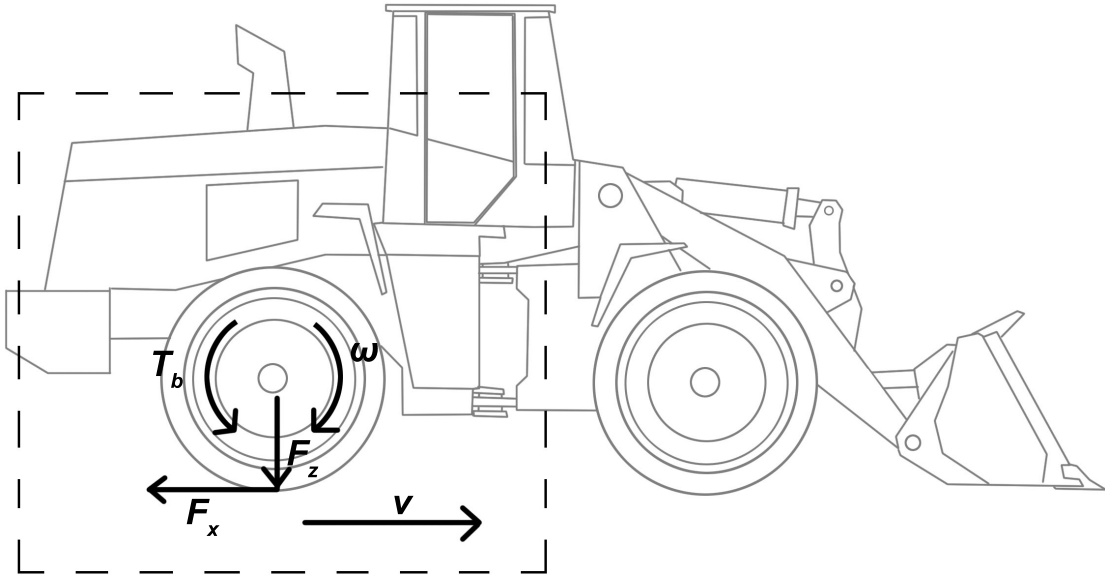


Figure 3.2. Single corner vehicle model

$$\begin{cases} \dot{\omega} = \frac{1}{J} (rF_x - T_b) \\ \dot{v} = \frac{-F_x}{m} \end{cases} \quad (3.2)$$

Where ω is the rotational velocity of the wheel, v is the longitudinal velocity of the vehicle, J is the wheel inertia, r is the wheel radius, T_b is the applied braking torque, F_x is the longitudinal friction force between the wheel and the ground, F_z is the normal force and m is the partial vehicle mass.

Substituting the relationship $F_x = F_z\mu(\lambda)$ together with (3.1) into (3.2) gives

$$\begin{cases} \dot{\omega} = \frac{1}{J} \left(rF_z\mu \left(\frac{v - \omega r}{v} \right) - T_b \right) \\ \dot{v} = \frac{-F_z\mu \left(\frac{v - \omega r}{v} \right)}{m} \end{cases} \quad (3.3)$$

Since the wheel slip, λ , is of interest it can be introduced as a state variable by taking the derivative of (3.1), giving

$$\dot{\lambda} = -\frac{\dot{\omega}rv - r\omega\dot{v}}{v^2} \quad (3.4)$$

Substituting $\dot{\omega}$ from (3.3) into (3.4) gives

$$\begin{cases} \dot{\lambda} = -\frac{1}{v} \left(\frac{1-\lambda}{m} + \frac{r^2}{J} \right) F_z \mu(\lambda) + \frac{r}{Jv} T_b \\ \dot{v} = \frac{-F_z \mu(\lambda)}{m} \end{cases} \quad (3.5)$$

3.2.1 Linearization and Equilibrium points

The augmented model derived in equation (3.5) can be linearized according to

$$\begin{aligned} \begin{bmatrix} \Delta \dot{\lambda} \\ \Delta \dot{v} \end{bmatrix} &= \begin{bmatrix} \left. \frac{\partial f_1}{\partial \lambda} \right|_{\lambda=\lambda_0, v=v_0} & \left. \frac{\partial f_1}{\partial v} \right|_{\lambda=\lambda_0, v=v_0} \\ \left. \frac{\partial f_2}{\partial \lambda} \right|_{\lambda=\lambda_0, v=v_0} & \left. \frac{\partial f_2}{\partial v} \right|_{\lambda=\lambda_0, v=v_0} \end{bmatrix} \begin{bmatrix} \Delta \lambda \\ \Delta v \end{bmatrix} + \begin{bmatrix} \frac{r}{J} \\ 0 \end{bmatrix} \Delta T_b \\ \Delta y &= C \begin{bmatrix} \Delta \lambda \\ \Delta v \end{bmatrix} \end{aligned} \quad (3.6)$$

where C is the output select matrix and

$$\begin{cases} f_1 = -\frac{1}{v} \left(\frac{1-\lambda}{m} + \frac{r^2}{J} \right) F_z \mu(\lambda) + \frac{r}{Jv} T_b \\ f_2 = \frac{-F_z \mu(\lambda)}{m} \end{cases} \quad (3.7)$$

Furthermore, the wheel slip equilibrium λ_0 will be placed somewhere to the left of the peak on the $\mu(\lambda)$ curve seen in Figure 3.1. The function $\mu(\lambda)$ can be simplified through the assumption that $\mu(\lambda)$ is a linear function of λ , that is $\mu(\lambda) = k\lambda$, this will render the state space

$$\begin{aligned} \begin{bmatrix} \Delta \dot{\lambda} \\ \Delta \dot{v} \end{bmatrix} &= \begin{bmatrix} -\frac{F_z k}{v_0} \left(\frac{1}{m} + \frac{r^2}{J} - \frac{2}{m} \lambda_0 \right) & \frac{F_z k}{v_0^2} \left(\left(\frac{1}{m} + \frac{r^2}{J} \right) \lambda_0 - \frac{1}{m} \lambda_0^2 \right) \\ -\frac{F_z k}{m} & 0 \end{bmatrix} \begin{bmatrix} \Delta \lambda \\ \Delta v \end{bmatrix} + \begin{bmatrix} \frac{r}{J} \\ 0 \end{bmatrix} \Delta T_b \\ \Delta y &= C \begin{bmatrix} \Delta \lambda \\ \Delta v \end{bmatrix} \end{aligned} \quad (3.8)$$

The transfer function from input to output can be computed as

$$G(s) = C(sI - A)^{-1}B \quad (3.9)$$

where

$$A = \begin{bmatrix} -\frac{F_z k}{v_0} \left(\frac{1}{m} + \frac{r^2}{J} - \frac{2}{m} \lambda_0 \right) & \frac{F_z k}{v_0^2} \left(\left(\frac{1}{m} + \frac{r^2}{J} \right) \lambda_0 - \frac{1}{m} \lambda_0^2 \right) \\ -\frac{F_z k}{m} & 0 \end{bmatrix} \quad (3.10)$$

$$B = \begin{bmatrix} \frac{r}{J} \\ 0 \end{bmatrix}$$

3.3 Dual corner vehicle model

The idea with the *Dual corner vehicle model* is to include the fact that the weight is transferred, or shifted, between the rear and front axle during braking. The weight shift will cause the contact forces on the wheels to change and thereby the tire-road friction.

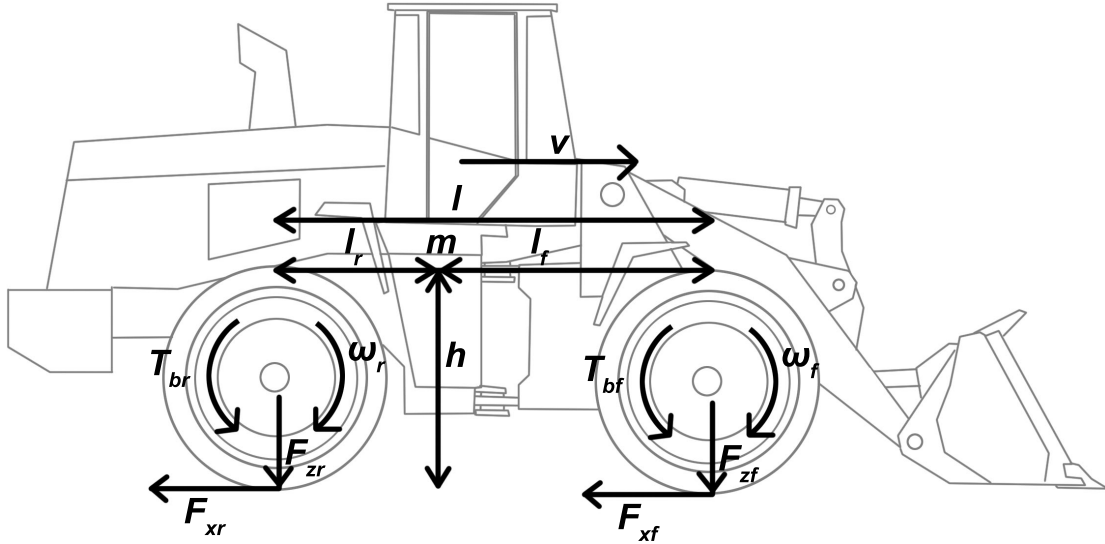


Figure 3.3. Dual corner vehicle model

The following set of equations can be derived from the free body diagram in Figure 3.3:

$$\begin{cases} \dot{\omega}_f = \frac{r}{J}F_{xf} - \frac{1}{J}T_{bf} \\ \dot{\omega}_r = \frac{r}{J}F_{xr} - \frac{1}{J}T_{br} \\ \dot{v} = -\frac{F_{xf}}{m} - \frac{F_{xr}}{m} \end{cases} \quad (3.11)$$

Where ω_f and ω_r are the rotational velocity of the front and rear wheel, respectively, v is the longitudinal velocity of the vehicle's center of mass, J is the wheel inertia, r is the wheel radius, T_{bf} and T_{br} is the applied braking torque on the front and rear wheel, respectively, F_{xf} and F_{xr} is the longitudinal friction force between the front respectively rear wheel and the ground.

Computing force and torque balance around the point where the mass m projects to the ground yields the following equations:

$$\begin{cases} mg = F_{zf} + F_{zr} \\ m\dot{v}h = F_{zr}l_r - F_{zf}l_f \end{cases} \quad (3.12)$$

where h is the vertical distance from the ground to the vehicle's center of mass, l is the wheelbase and l_f and l_r is the horizontal distance from the front and rear axis, respectively, to the vehicle's center of mass.

Solving (3.12) for F_{zf} and F_{zr} gives

$$\begin{cases} F_{zf} = F_{zfs} + \Delta_{F_z} \dot{v} \\ F_{zr} = F_{zrs} + \Delta_{F_z} \dot{v} \end{cases} \quad (3.13)$$

Where

$$\begin{cases} F_{zfs} = \frac{mgl_r}{l} \\ F_{zrs} = \frac{mgl_f}{l} \end{cases} \quad (3.14)$$

are the static normal forces on the front and rear axis, respectively, and

$$\Delta_{F_z} = \frac{mh}{l} \quad (3.15)$$

is the dynamic change in normal force due to the weight shift during braking.

The wheel slip λ_i , $i = \{f, r\}$ can be introduced as state variables using the same analogy as in the single corner model. Substituting the relationship $F_{xi} = F_{zi} \cdot \mu(\lambda_i)$, $i =$

$\{f, r\}$ together with (3.13), (3.4) and ω_i , $i = \{f, r\}$ from (3.11). Furthermore, \dot{v} can be rewritten using (3.1) together with (3.13) and $F_x = F_z \mu(\lambda)$ which will render the system model

$$\begin{cases} \dot{\lambda}_f = -\frac{r}{Jv} \left(r (F_{zfs} - \Delta_F \dot{v}) \mu(\lambda_f) - \frac{J}{r} (1 - \lambda_f) \dot{v} - T_{bf} \right) \\ \dot{\lambda}_r = -\frac{r}{Jv} \left(r (F_{zrs} + \Delta_F \dot{v}) \mu(\lambda_r) - \frac{J}{r} (1 - \lambda_r) \dot{v} - T_{br} \right) \\ \dot{v} = -\frac{F_{zfs} \mu(\lambda_f) + F_{zrs} \mu(\lambda_r)}{m - \Delta_F (\mu(\lambda_f) - \mu(\lambda_r))} \end{cases} \quad (3.16)$$

The vehicle model can be extended with a model of the hydraulic part of the actuator, which was based on the assumptions given by [15]. The transfer function is presented in equation 3.17, where $T_d = 0.02$ s.

$$G_{hydraulic} = \frac{60e^{-T_d s}}{s + 60} \quad (3.17)$$

3.4 Anti Lock system

There are typically two main approaches to design an anti lock controller. The first one is to control the amount of wheel slip on the wheel and the other one is to control the wheel deceleration. One of the (most) beneficial factors of a wheel slip controller is that it is quite easy to find a set-point that will yield good performance at almost any surface, since the peak of the friction curve for different surfaces lies very close to each other with respect to λ , see Figure 3.1 [15]. This makes the slip controller very robust and no estimation of the surface is needed to give a good brake performance. However both measurement of the vehicle speed and the angular speed of the wheels are needed and the wheel slip λ is very sensitive to noise, especially at low speeds.

With wheel deceleration the surface has to be known i.e measured or estimated since the amount of (maximum) deceleration depends on the surface. A wheel deceleration controller lacks the robustness of the slip controller due to the fact that reference set-point could be set higher than what the vehicle could produce on the current surface. A scenario like this will lead to that there is no solution to the set-point and the controller will eventually lock the wheels. This problem could be solved by decreasing the set-point, however it might lead to an overly conservative controller. Although the wheel deceleration poses some problems with stability, i.e feasible set-points, it has some attractive features. It only needs the wheel speed and surface estimation. The vehicle velocity is often measured with the rotation of the wheels so in these cases no extra sensors are needed, although extra sensors might be needed to estimate the surface.

Due to the robust properties of the wheel slip controller, it was decided that the

controller will be of this type.

3.5 Wheel slip model

Equation 3.5 shows that the rate of change of the wheel slip, $\dot{\lambda}$, depends on the vehicle speed. However the dynamics of the vehicle is far slower than the dynamics of the wheel slip, thus the vehicle speed can be considered slowly varying, i.e constant around a linearization point at an equilibrium point of λ [15]. With this assumption, the second equation in 3.5 is not included in the linearization process. At some linearization point the wheel slip and torque are defined as:

$$\Delta\lambda = \lambda - \lambda_0, \Delta T_b = T_b - T_{b0} \quad (3.18)$$

$$\Delta\dot{\lambda} = \frac{Fz}{\bar{v}} \left(\frac{\mu(\lambda_0)}{m} - \mu_1(\lambda_0) \left(\frac{(1-\lambda_0)}{m} + \frac{r^2}{J} \right) \right) \Delta\lambda + \frac{r}{J\bar{v}} \Delta T_b \quad (3.19)$$

This gives the transfer function from torque to wheel slip as:

$$G_{wheel\ slip} = \frac{\Delta\lambda}{\Delta T_b} = \frac{\frac{r}{J\bar{v}}}{s + \frac{Fz}{\bar{v}} \left(\frac{\mu(\lambda_0)}{m} - \mu_1(\lambda_0) \left(\frac{(1-\lambda_0)}{m} + \frac{r^2}{J} \right) \right)} \quad (3.20)$$

3.6 Brake actuator

The brake actuator is a solenoid valve as described in Chapter 2.1.3. A solenoid can be seen as a inductor and a resistor connected in series. Such a system is a first order linear time invariant system and the transfer function from input voltage V_{in} to output current I_{out} can be modeled as:

$$G_{V_{in}I_{out}}(s) = \frac{K}{s\tau + 1} \quad (3.21)$$

where K is the steady state gain and τ is the system's time constant defined as the time it takes for the system to reach $1 - 1/e \approx 63.2\%$ of the steady state output value.

These parameters can be acquired through step test analysis. Figure 3.4 shows the actuator current response when a 14 V signal was applied at time $t = 10$ ms. The actuator steady state current output is approximately 0.65 A and the actuator's time constant τ can be approximated to $\tau \approx 15$ ms. Thus giving the system's transfer function as:

$$G_{V_{in}I_{out}}(s) = \frac{13/280}{0.015s + 1} \quad (3.22)$$

The nudge seen in Figure 3.4 at around $t = 15$ ms is considered to be due to solenoid stiction and has been neglected.

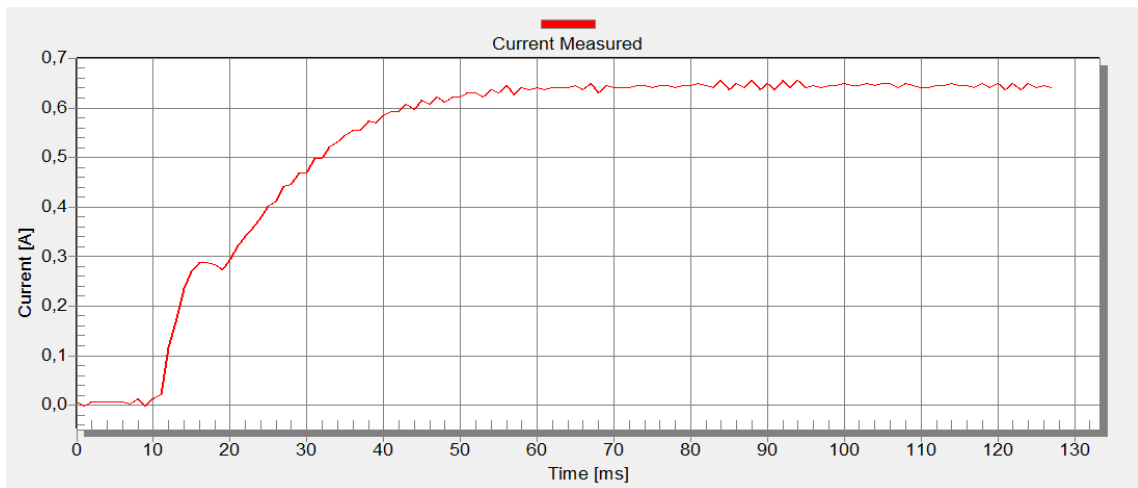


Figure 3.4. Step response of brake actuator

4 Controller Design

This chapter describes the design of the entire brake control system. A functional schematic is presented in Figure 4.1. The brake system can either take input from the *brake pedal* to the *brake pedal controller* or a reference of desired vehicle acceleration from the *driveline control* to the *retardation controller*. Both of these controllers calculates a desired brake torque which is then fed to a *controller selector* which choses what controller output that shall be passed through. The *retardation controller* is activated through a CAN message and the *brake pedal* is always active and has the highest priority. The selected controller output is then fed to an *anti-lock controller* which makes sure that the requested torque and the wheel slip are not too high, if so the *anti-lock controller* will limit the brake torque. The final brake torque is then fed to the *actuator controller*, which controls the brake pressure in the brake circuit. A *state observer*, described in Chapter 2.2.3, will provide filtered state data to the *anti-lock controller* and the *retardation controller*. Due to the fact that there are several controllers and switching between these the brake controller has bumpless transfer and anti wind up algorithms to ensure that the transitions between the controllers are smooth.

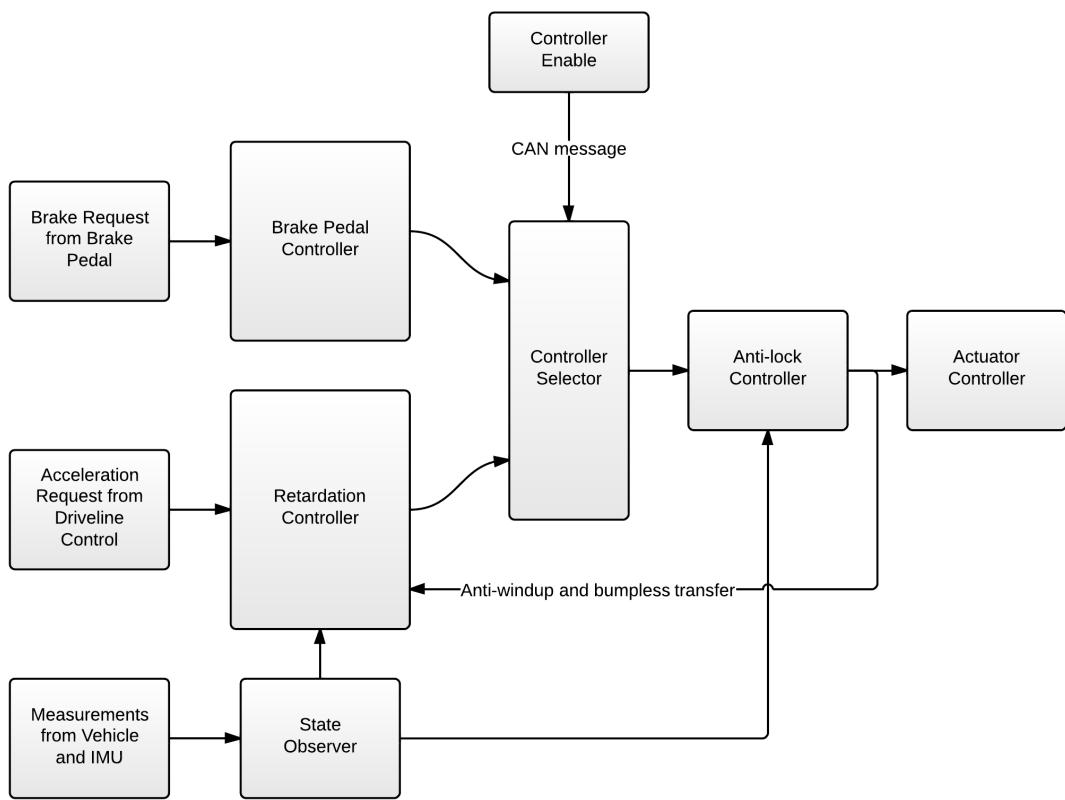


Figure 4.1. Controller overview

4.1 Actuator Controller

The design methodology of the actuator controller was influenced by the Ziegler-Nichols method because the actuator could easily be tested and the method yields good disturbance rejection [13].

The measured current is sampled at the midpoint of the PWM positive pulse, this is to minimize the electrical transients from the positive PWM flank. Integral windup is prevented by saturating the output in software and adding a circuit similar to the one described in Chapter 4.5.

A problem with controlling solenoid valves is that the plunger needs to overcome the static friction before it starts to move, this phenomenon is called stiction. Stiction can cause issues where the current through the solenoid is increased by a tiny factor but the plunger does not move, leaving the pressure output from the valve unchanged. One simple method to counteract this is to add a varying control signal, typically a sine wave, so that the control signal is never constant, this is called dithering. The frequency of the added control signal should be chosen such that it is slow enough for the plunger to move but fast enough so that the contribution from the added control signal is attenuated by the actuator dynamics.

4.2 Brake Pedal Controller

The Brake Pedal Controller will essentially function as an open-loop quantizer with the only constraint that the input-output behavior, from an electrical voltage input to requested brake torque, has to be monotonically increasing. The input-output mapping is designed in such a way that the rate change on the output is increasing towards the end of the pedal stroke. This design is chosen based on the assumption that the driver is more likely to be in a panic brake situation if the pedal is pushed far into its stroke. The controller has a slight overhead in control signal compared to what the system can deliver, this is to assure that maximum braking torque is always delivered if the pedal is pressed to the floor despite any local vehicle variations. Two examples of input-output mappings are shown in Figure 4.2, where the left graph shows a linear mapping and the right shows a progressive.

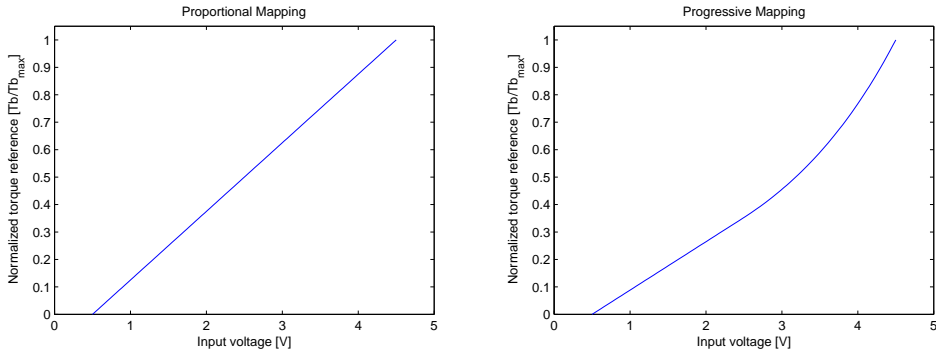


Figure 4.2. Brake pedal controller input-output mapping, *left*: linear mapping, *right*: progressive mapping

4.3 Retardation Controller

The requirement set on the retardation controller is that it should be fast but without overshooting, i.e. the system should be damped. This is because the perceived braking should feel smooth, and to create a good robustness against disturbances and model inaccuracies. Due to its simplicity and disturbance robustness, a PI-controller was designed

The transfer function for a PI-controller takes the form

$$F_{PI}(s) = \frac{K_p s + K_i}{s} \quad (4.1)$$

where K_p is the proportional gain and K_i is the integral gain.

The linearized plant model derived in Chapter 3.2.1 can be expressed on the form

$$G(s) = \frac{as}{s^2 + bs + c} \quad (4.2)$$

where a , b and c can be identified from

$$G(s) = C(sI_2 - A)^{-1}B \quad (4.3)$$

where

$$\begin{aligned}
A &= \begin{bmatrix} -\frac{F_z k}{v_0} \left(\frac{1}{m} + \frac{r^2}{J} - \frac{2}{m} \lambda_0 \right) & \frac{F_z k}{v_0^2} \left(\left(\frac{1}{m} + \frac{r^2}{J} \right) \lambda_0 - \frac{1}{m} \lambda_0^2 \right) \\ -\frac{F_z k}{m} & 0 \end{bmatrix} \\
B &= \begin{bmatrix} \frac{r}{J} \\ 0 \end{bmatrix} \\
C &= \left[-\frac{F_z k}{m} \quad 0 \right]
\end{aligned} \tag{4.4}$$

The much faster dynamics in the actuator will be handled by the actuator controller and is therefore not taken into account when synthesizing the retardation controller.

The closed-loop transfer function for the system takes the form

$$G_{ry} = \frac{F(s)G(s)}{F(s)G(s) + 1} = \frac{K_p a s + K_i a}{s^2 + (K_p a + b)s + (K_i a + c)} \tag{4.5}$$

Equation (4.5) can be compared with the standard equation for a second order system with a zero:

$$G(s) = \frac{\left(\frac{s}{z} - 1 \right) K_\infty \omega_c^2}{s^2 + 2\zeta \omega_c s + \omega_c^2} \tag{4.6}$$

where ζ is the damping ratio, ω_c is the closed-loop system's crossover frequency, K_∞ is the open-loop gain and z is the system's zero.

The controller parameters can be identified as

$$\begin{cases} K_p = \frac{2\zeta \omega_c - b}{a} \\ K_i = \frac{\omega_c^2 - c}{a} \end{cases} \tag{4.7}$$

which will render a zero in

$$z = -\frac{\omega_c^2 - c}{2\zeta \omega_c - b} \tag{4.8}$$

The damping ratio, ζ , is set to 1 to render critical damping. The plant's undamped natural frequency, ω_n can be found by comparing (4.2) with (4.6), this gives $\omega_n = \sqrt{c}$.

The sensitivity function,

$$S(s) = \frac{1}{F_{PI}(s)G(s) + 1} \tag{4.9}$$

is presented in Figure 4.3. This transfer function can be interpreted as the transfer function from load disturbances to the output. Intuitively, high controller gain will render better robustness against load disturbances. Figure 4.3 shows how high gain, i.e. high ω_c , gives a greater attenuation of load disturbances.

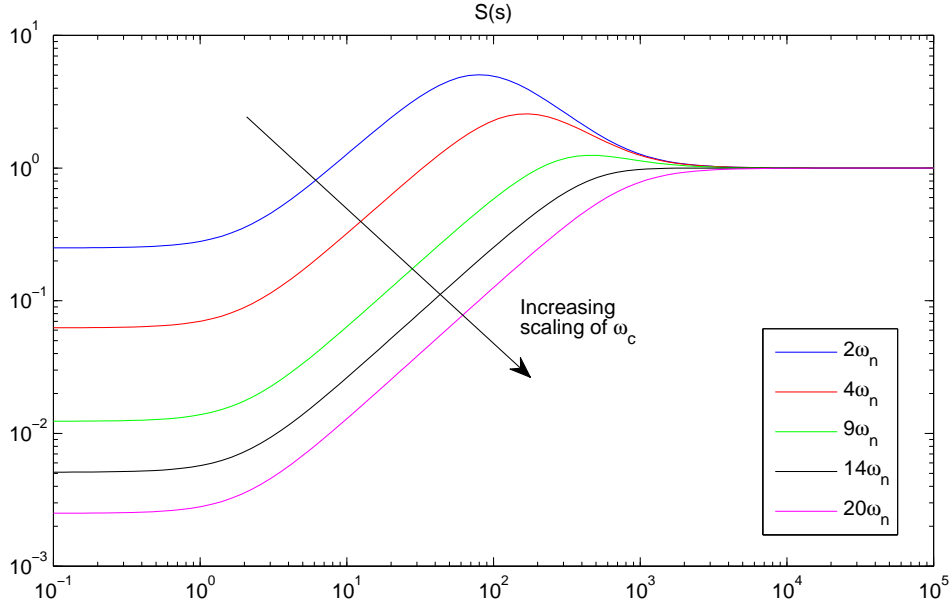


Figure 4.3. The sensitivity function's frequency response for different scaling of ω_c

The complementary sensitivity function, described as

$$T(s) = \frac{F_{PI}(s)G(s)}{F_{PI}(s)G(s) + 1} \quad (4.10)$$

can be interpreted as the transfer function from measurement noises to the output. From the frequency response, shown in Figure 4.4, one can notice how increasing ω_c will result in an attenuation of the lump at around $\omega = 10^2$ rad/s, but also for larger ω_c the gain is increased for higher frequencies.

ω_c was chosen as

$$\omega_c = 10\omega_n \quad (4.11)$$

which was considered a good compromise between influence of load disturbances and measurement noise.

The amplitude and phase margins, A_m and φ_m respectively, are guaranteed to be

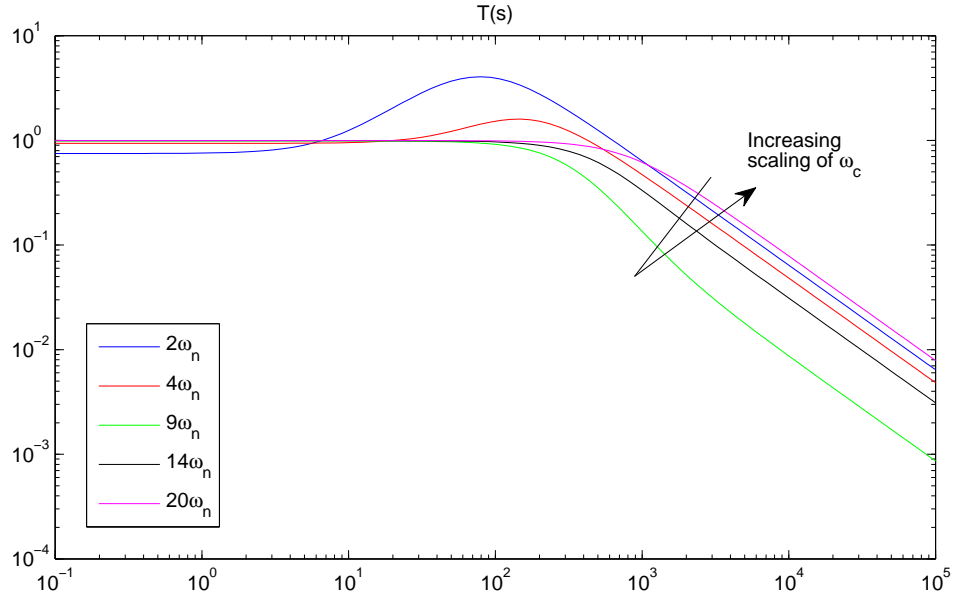


Figure 4.4. The complementary sensitivity function's frequency response for different scaling of ω_n

$$A_m \geq \frac{M_S}{M_S - 1} \quad (4.12)$$

$$\varphi_m \geq 2 \arcsin \left(\frac{1}{2M_T} \right)$$

where $M_S = \max_{\omega} |S(j\omega)|$ and $M_T = \max_{\omega} |T(j\omega)|$. [5]

Which for this particular closed-loop system would yield an amplitude- and phase margin of

$$A_m \geq 7.31 \quad (4.13)$$

$$\varphi_m \geq 60.7^\circ$$

Figure 4.5 shows the frequency response of the complementary sensitivity function, the sensitivity function and the open-loop transfer function for the feedback system.

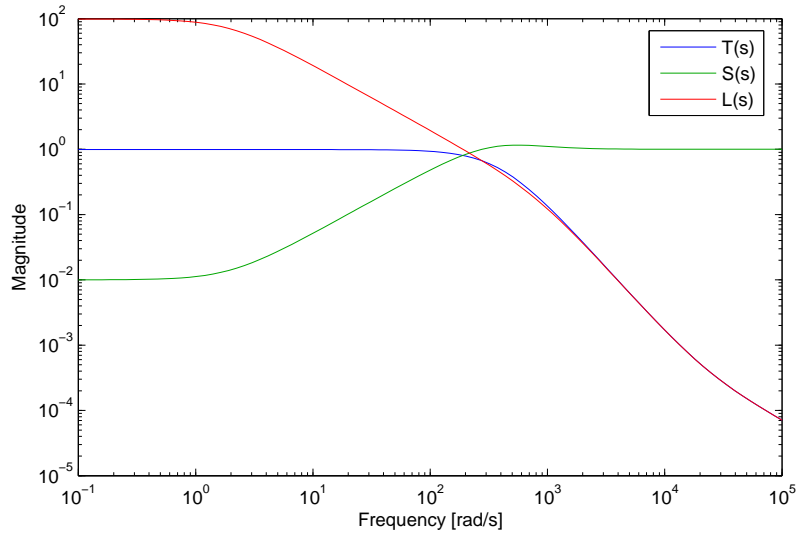


Figure 4.5. Frequency response of the complementary sensitivity function $T(s)$, the sensitivity function $S(s)$ and the open-loop transfer function $L(s)$

4.4 Anti-lock system

As described in Section 2.2.2 the anti-lock system's task is to assure that the wheels do not lock and that the slip is kept at a near optimal value. Figure 4.6 shows an overview of the anti-lock system. The controller takes the requested braking torque from the brake controller, $T_{b,req}$, the current wheel slip, λ , and the current vehicle velocity, v , as input. The output torque is fed back to the brake controller to allow for anti-windup and bumpless switching between controllers.

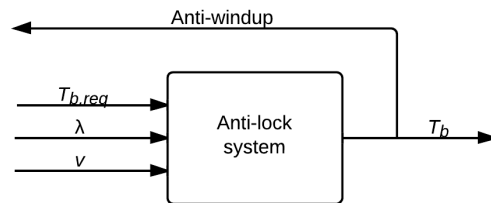


Figure 4.6. Overview of the anti-lock module

4.4.1 Wheel Slip Control

The requirement set on the wheel slip controller is that it should be fast enough to prevent the wheels from locking without too much overshoot, i.e. the system should be well damped. This is important since there will be switches between the

brake pedal controller and retardation controller to the slip controller. Switching between controllers can often lead to unexpected behavior and stability is often hard to prove, thus to compensate and have a little headroom against reduced stability margins it is important to have a well damped system. For simplicity reasons the controller was designed based on the single corner model and for the same reason a PI controller structure was used.

$$F_{PI}(s) = \frac{K_p s + K_i}{s} \quad (4.14)$$

The vehicle transfer function is given by Laplace transformation of equation 3.19.

$$G_\lambda = \frac{r}{J\bar{v}} \frac{1}{s + \frac{F_z \mu_1(\bar{\lambda})}{m\bar{v}} \left((1 - \bar{\lambda}) + \frac{mr^2}{J} \right)} \quad (4.15)$$

For readability the parameters are lumped together as the following

$$\begin{aligned} \alpha &= \frac{r}{J\bar{v}} \\ \beta &= \frac{F_z \mu_1(\bar{\lambda})}{m\bar{v}} \left((1 - \bar{\lambda}) + \frac{mr^2}{J} \right) \\ G_\lambda &= \frac{\alpha}{s + \beta} \end{aligned}$$

To the right of the peak of the friction curve the system will be open-loop unstable since $\mu_1 < 0$ which gives a pole in the right half plane (RHP). The controller parameters must therefore be chosen such that the closed-loop system is stable in every operating point. To ensure that the controller manages to stabilize the system a worst case operating point has to be found to determine the stability condition. Figure 4.7 illustrates the pole location with respect to wheel slip for different surfaces. A wheel slip of 0.87 on cobblestone results in a pole in the RHP which is furthest away from the imaginary axis. However according to [15] this amount of wheel slip on cobblestone is very unlikely to happen. From simulation results presented in Chapter 6, it was shown that for a wheel loader a wheel slip over 0.16 is not very likely to occur. Therefore the worst case amount of wheel slip was set to this value, which will further on be referred to as λ_{crit} .

The poles to the system are given by the characteristic equation

$$F(s)G(s) + 1 = 0 \quad (4.16)$$

which yields

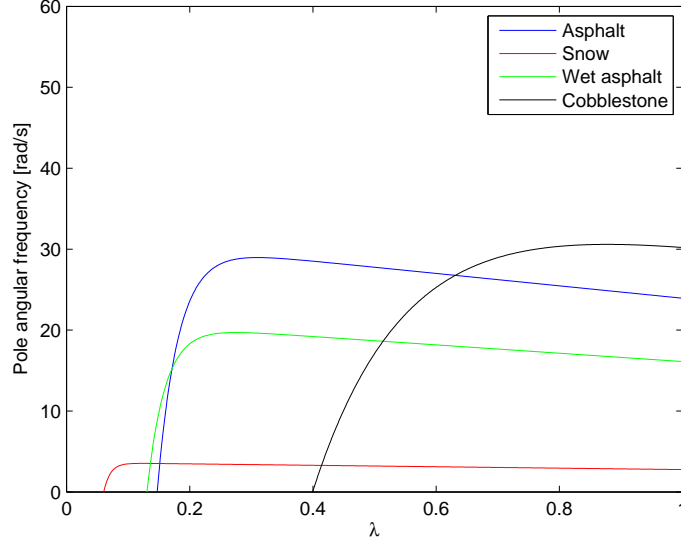


Figure 4.7. Open-loop pole location with respect to wheel slip and surface normalized with the vehicle speed

$$\alpha(K_p s + K_i) + s(s + \beta) = 0 \quad (4.17)$$

which according to *Routh Hurwitz* stability criterion [5] gives the stability conditions

$$\begin{cases} K_p > \frac{\beta}{\alpha} \\ K_i > 0 \end{cases} \quad (4.18)$$

The parameter β is the pole of the linearized system. Since the system needs to be stable in every reasonable and foreseeable operating point the lower bound of the parameter K_p is set according to 4.18 with β equal the pole at $\lambda = \lambda_{crit}$. The controller will then be designed such that it manages to stabilize the system when the pole is located in the RHP with $\lambda = \lambda_{crit}$. The closed-loop system is given by

$$G_{ry} = \frac{F(s)G(s)}{F(s)G(s) + 1} = \frac{L(s)}{L(s) + 1} = \frac{(K_p s + K_i)\alpha}{(K_p s + K_i)\alpha + s(s - \beta)} \quad (4.19)$$

Since it is desirable that the system is well damped and since it is a second order polynomial, a real double pole is achieved by identifying the closed-loop with the standard polynomial

$$\frac{K_i + K_p s}{(s + \omega_n)^2} \quad (4.20)$$

This gives

$$\begin{aligned}\omega_n &= \sqrt{K_i \alpha} \\ K_p &= \frac{2\sqrt{\omega_n} + b}{a}\end{aligned}\tag{4.21}$$

As rule of thumb, the phase margin, φ_m , should be $> 45^\circ$ in order to achieve a well damped system and this generally gives good stability margins [5]. The phase margin, φ_m , is the amount that the phase shift can be increased at the crossover frequency, ω_c , before the system becomes unstable and is defined as:

$$\varphi_m = \angle L(j\omega_c) + 180^\circ\tag{4.22}$$

To achieve this, the controller $F(S)$ can be extended to a PID controller. The derivative gain K_d is then iterated numerically until a phase margin, φ_m of $> 45^\circ$ is achieved. The results of the PID controller is presented in Chapter 6.

4.4.2 Anti-lock System Activation and Deactivation

The activation and deactivation logic is presented in Figure 4.8. The anti-lock system is activated if the wheel slip exceeds a certain threshold, if the slip controller requests lower torque output than the brake controller and if the velocity is above a certain threshold. Since stability issues might occur at low speed the anti-lock system is only allowed to operate above a certain velocity threshold. All transitions use hysteresis to prevent unwanted rapid switching.

The parameters in Figure 4.8 are defined in Table 4.1.

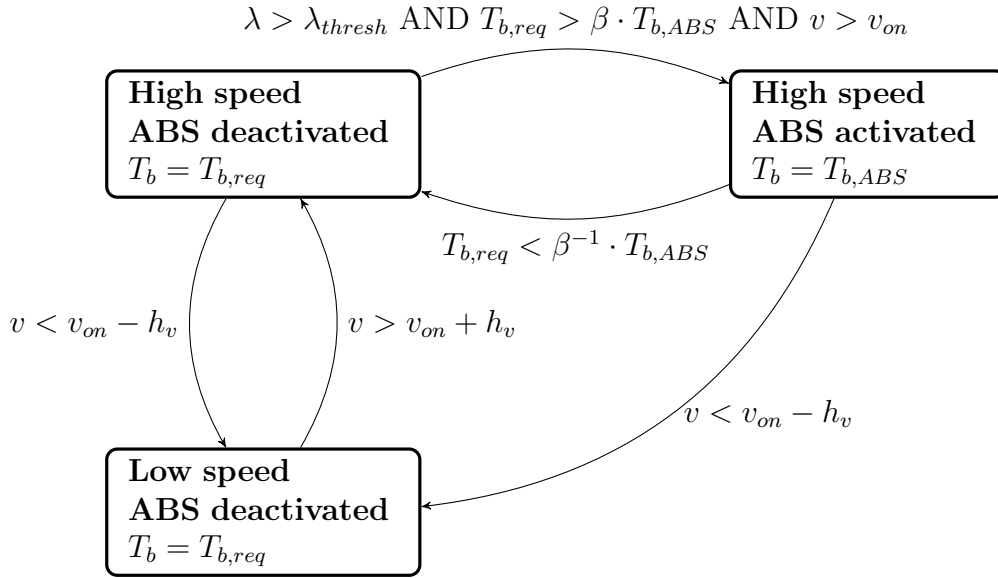


Figure 4.8. Controller overview

Table 4.1. Anti-lock system parameters

Variable	Typical value	Description
T_b		Braking torque output from anti-lock system.
$T_{b,req}$		Requested braking torque form brake controller.
$T_{b,ABS}$		Requested braking torque from anti-lock controller.
λ		Wheel slip.
v		Vehicle velocity.
Constant		
λ_{thresh}	~ 0.07	Slip threshold.
β	> 1	Braking torque proportional hysteresis.
h_v	> 0	Velocity additive hysteresis.
v_{on}	~ 2 m/s	Velocity threshold where the anti-lock system is activated or deactivated.

4.5 Anti-windup and bumpless switching between controllers

When running several controllers in parallel, where only one of them controls the actual output, it is important that the controller outputs coincide at the time of switching to allow for smooth operation. This is called "bumpless transfer".

An issue with integral controllers is that they will wind up if either the control

signal is saturated outside the controller, or if an other controller is controlling the plant. Fortunately both anti-wind up and smooth transitions between the controllers can be solved with a bumpless transfer circuit. Such a circuit will assure that the controller's integral output follows the actual output from the control system, by adding or removing quantities from the integrator depending on whether the controller's output is smaller or larger than the actual control output.

Figure 4.9 shows the implementation of a bumpless transfer circuit, where

- **Control_error** is the control error.
- **Controller_output** is the control signal from the controller itself.
- **Actual_control_output** is the actual control signal given by the controller which is currently controlling the actual plant.

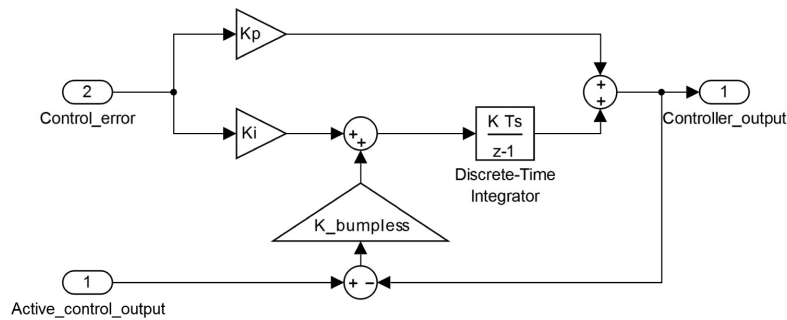


Figure 4.9. PI-controller with bumpless transfer

The circuit basically compares the output generated by the controller and the actual output at the end at the controller scheme, i.e the output generated to the actuator. If these are not equal, then either the output from the controller is saturated or some other controller is generating the actual control output. To prevent the integrating part from correcting this non error the difference is multiplied with a gain which decreases the integrating part. As a rule of thumb, [12], the bumpless transfer gain should be decided such that

$$K_{bumpless} > \frac{1}{T_i} \left(= \frac{K_i}{K_p} \right) \quad (4.23)$$

This means that the gain is faster than the time constant of the integrating part, which means that the integrating part will decrease.

4.6 State Observer

As described in Chapter 2.2.3 it is desirable that many of the vehicle's non measurable states are available. A common approach to acquire these is to use a so called

Kalman filter, also known as linear quadratic estimator [4]. The nonlinear dynamics of the vehicle requires the extended version of the Kalman filter.

4.6.1 Extended Kalman Filter

The Extended Kalman Filter will estimate a system on the form

$$\begin{cases} x_k = f(x_{k-1}, u_{k-1}) + w_{k-1} \\ y_k = h(x_{k-1}) + v_{k-1} \end{cases} \quad (4.24)$$

where w and v are the process and measurement noise, respectively, with covariance Q and R , respectively. These noises are assumed to be zero mean multivariate Gaussian noise to make the Kalman filter applicable. Subscript k denotes a point in discrete time and $k - 1$ denotes the prior point in discrete time.

The filter uses a predict and update algorithm according to:

Prediction

$$\begin{aligned} \text{Predict state estimate} \quad \hat{x}_{k|k-1} &= f(\hat{x}_{k-1|k-1}, u_{k-1}) \\ \text{Predict covariance estimate} \quad P_{k|k-1} &= F_{k-1} P_{k-1|k-1} F_{k-1}^T + Q \end{aligned}$$

Update

$$\begin{aligned} \text{Measurement residual} \quad \tilde{y} &= y_k - h(\hat{x}_{k|k-1}) \\ \text{Residual covariance} \quad S_k &= H_k P_{k|k-1} H_k^T + R \\ \text{Near-optimal Kalman gain} \quad K_k &= P_{k|k-1} H_k^T S_k^{-1} \\ \text{Updated state estimate} \quad \hat{x}_{k|k} &= \hat{x}_{k|k-1} + K_k \tilde{y} \\ \text{Updated covariance estimate} \quad P_{k|k} &= (I - K_k H_k) P_{k|k-1} \end{aligned}$$

where P is the covariance estimate, y is the measured quantity, S is the residual covariance, K is the near-optimal Kalman gain, $k|k - 1$ denotes an estimate of time k based on data from time $k - 1$, F_{k-1} and H_k are the Jacobians of f and h respectively, defined as

$$F_{k-1} = \left. \frac{\partial f}{\partial x} \right|_{\hat{x}_{k-1|k-1}, u_{k-1}} \quad (4.25)$$

$$H_k = \left. \frac{\partial h}{\partial x} \right|_{\hat{x}_{k|k-1}} \quad (4.26)$$

Discretization

The vehicle dynamics model derived in Chapter 3.3 is a set of time continuous equations. However, the system need to be discretized due to the fact that the extended Kalman filter is a discrete filter.

A simple approach for discretization is using the Forward Euler method. Any system of the form

$$\dot{x}(t) = f(x(t)) \quad (4.27)$$

can be discretized using the Forward Euler method to

$$x_{k+1} = x_k + h \cdot f(x_k) \quad (4.28)$$

where h is the sample time.

When discretizing the model one should keep in mind what the intended outcome of the observer is and thereby choose the states wisely. The observer states for this particular application was chosen as

$$\hat{x} = \left[\hat{\omega}_f \quad \hat{\omega}_r \quad \hat{v} \quad \hat{\lambda}_f \quad \hat{\lambda}_r \quad \hat{\mu}_f \quad \hat{\mu}_r \right]^T \quad (4.29)$$

Which according to (4.28) and (3.16) will yield the following discretized model:

$$\left\{ \begin{array}{l} \omega_f(k) = \omega_f(k-1) + h \frac{1}{J} \left(r \mu_f(k-1) \left(\frac{mgl_r}{l} - \frac{mh}{l} \cdot W(k-1) \right) - T_{bf} \right) \\ \omega_r(k) = \omega_r(k-1) + h \frac{1}{J} \left(r \mu_r(k-1) \left(\frac{mgl_f}{l} + \frac{mh}{l} \cdot W(k-1) \right) - T_{br} \right) \\ v(k) = v(k-1) + h \cdot W(k-1) \\ \lambda_f(k) = \frac{v(k-1) - r\omega_f(k-1)}{v(k-1)} \\ \lambda_r(k) = \frac{v(k-1) - r\omega_r(k-1)}{v(k-1)} \\ \mu_f(k) = \nu_1 (1 - e^{-\nu_2 \lambda_f(k-1)}) - \nu_3 \lambda_f(k-1) \\ \mu_r(k) = \nu_1 (1 - e^{-\nu_2 \lambda_r(k-1)}) - \nu_3 \lambda_r(k-1) \end{array} \right. \quad (4.30)$$

Where

$$W(k) = -\frac{g(\mu_f(k)l_r + \mu_e(k)l_f)}{l + H(\mu_r(k) - \mu_f(k))} \quad (4.31)$$

The time indexes are placed as argument in (4.30) and (4.31) to improve readability.

5 ISO-26262 Theory

Risk analysis is important since the brake system is a safety critical system. Malfunctions in the brake system could lead to lethal risk for people in the vehicle's surrounding, which is not acceptable, thus the brake system must have a high reliability. The ISO-26262 is a standard developed by the automotive industry with the purpose to give guidelines, methods and evaluation tools to ensure, or maximize the probability that a system is safe.

5.1 ISO 26262

ISO 26262 is a development of the IEC 61508 standard targeted towards electronic and embedded systems in passenger cars. This brake by wire system will be integrated on construction vehicles such as articulated haulers or wheel loaders. A full analysis according to ISO-26262 is quite extensive and will therefore, as mentioned previously, not be performed. This thesis will cover the fundamentals of the ISO framework and work will be performed as in Figure 5.1, which is based on the concept phase given in [7].

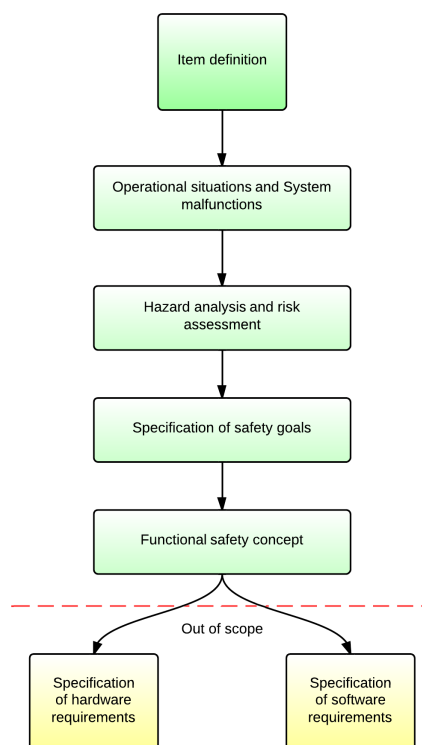


Figure 5.1. The project work-flow of the ISO-26262 analysis

5.1.1 Item definition

The purpose with the item definition is to specify and identify what part of the whole system that should be analyzed and what interactions and dependencies the item has.

5.1.2 Hazard analysis and Risk Assessment

In the hazard analysis and risk assessment different malfunctions are identified were the item could endanger the safety of people. Several scenarios are created for each malfunction occurring at different operational situations, these are referred to as a hazardous events. Each hazardous event is then analyzed with respect to three subparts; Controllability, Exposure and Severity [8]. Each of these subparts are graded according to Table 5.1, Table 5.2 and Table 5.3, respectively. The classification of severity is based on the abbreviated injury scale (AIS), presented in Table 5.4. The grades of these subparts are then combined which gives an Automotive Safety Integrity Level (ASIL) which acts as a total score for the hazardous event. This ASIL level will serve as a base when deciding the technical safety requirements on the system.

Table 5.1. Classification of controllability

C0	C1	C2	C3
Controllable in general	Simply controllable (99% or more of all drivers or other traffic participants are usually able to avoid a specified harm)	Normally controllable (90% or more of all drivers or other traffic participants are usually able to avoid a specified harm)	Difficult to control or uncontrollable (Less than 90% of all drivers or other traffic participants are usually able, or barely able, to avoid a specified harm)

Table 5.2. Classification of exposure

	E1	E2	E3	E4
Duration	Not specified	< 1% of average operating time	1% to 10% of average operating time	> 10 % of operating time
Frequency of situation	Occurs less often than once a year for the great majority of drivers	Occurs a few times for the great majority of drivers	Occurs once a month or more often for an average driver	Occurs during almost every drive at average

Table 5.3. Grading of Severity

S0	S1	S2	S3
AIS 0 and less than 10% of AIS 1-6	More than 10 % probability of AIS 1-6	More than 10 % probability of AIS 3-6	More than 10 % probability of AIS 5-6

Table 5.4. Classification and identification of Abbreviated Injury Scale (AIS)

AIS 0	No injuries
AIS 1	Light injuries,e.g skin-deep wounds, muscle pains, whiplash
AIS 2	Moderate injuries, deep flesh wounds, concussion, light bone fractures
AIS 3	Severe but not life threatening injuries, skull fractures with no brain damage
AIS 4	Severe injuries, life threatening but survival probable
AIS 5	Critical injuries, survival uncertain, intestinal tears, cardiac tears
AIS 6	Extremely critical injuries, extremely critical open wounds

5.1.3 Safety Goals

All hazardous events with a classification of ASIL A or higher must be prevented from occurring. To achieve this, safety goals are created, each mapping to one specific hazardous events. The safety goals are defined according to Table 5.5. The ASIL of the safety goal is given by the ASIL of the hazardous event. If the hazardous event can not be prevented, each safety goal must be equipped with a safe state where the malfunction cannot affect the item. Furthermore, the maximum time allowed from when a malfunction occurs until the item has reached a safe state needs to be specified, this is referred to as fault tolerant time. Two or more safety goals can be combined into one, the ASIL classification is inherited from the safety goal that has the highest ASIL level.

Table 5.5. Generic classification of safety goals

Safety Goal	Highest ASIL	Safe State	Fault tolerant time
safety goal A	ASIL X	state Y	xx ms

5.1.4 Functional Safety Concept

The functional safety concept will identify all errors that will lead to a violation of any of the safety goal. This is preferably done with a Fault Tree Analysis (FTA). All errors identified in the tree that violates the safety goal are given the same ASIL as the safety goal. It is possible to decompose the ASIL level if the violation of a safety goal depends on several errors occurring at the same time, and those errors are independent of each other.

6 System Test and Results

This chapter describes the test scenarios and the test results.

6.1 Simulations

Simulations on all the system's subparts, presented in Chapter 2.2, were conducted. The subparts were tested on the dual corner vehicle model and the physical parameters used in all simulations are found in Table 6.1¹. The controllers were designed for the single corner vehicle model, described in Chapter 3.2, but verified on the enhanced dual corner vehicle model with actuator dynamics, described in Chapter 3.3.

Table 6.1. Simulation parameters

Parameter	Value	Description
h	.5 m	Length from center of mass to ground
l_f	1 m	Horizontal distance from center of mass to front wheel
l_r	.6 m	Horizontal distance from center of mass to rear wheel
l	1.6 m	Total vehicle length
λ_{sp}	0.08	Wheel slip setpoint
m	2000 kg	Quarter vehicle's mass
m_{wheel}	100 kg	Wheel's mass
r	0.5 m	Wheel radius
g	9.81 m/s ²	Gravitational constant
v_0	10 m/s	Initial velocity
$\mu(\lambda)$	-	Surface is dry asphalt

6.1.1 Vehicle model

The vehicle model derived in Chapter 3.3 was step tested with a 3.1 kNm torque applied at time $t = 1$ s, the open-loop torque step response is shown in Figure 6.1. The system's time constant is identified as $\tau \approx 25$ ms and the system's dead time is indeed 20 ms.

¹Variations in parameter value might apply for different simulations, these are stated in the corresponding subchapter

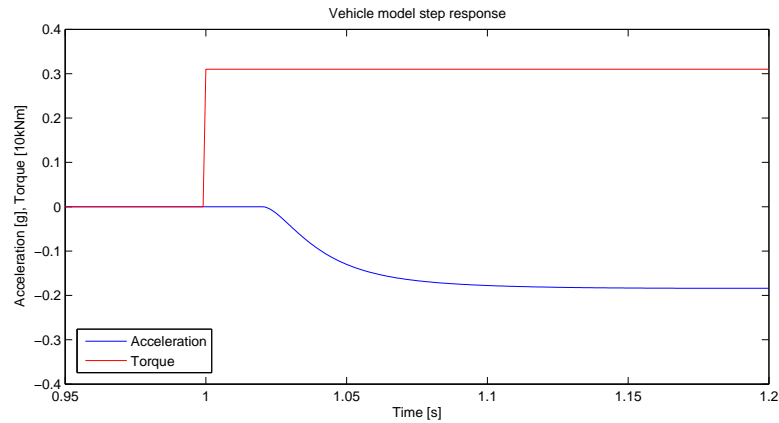


Figure 6.1. Vehicle step response

6.1.2 Wheel Slip Analysis

Figure 6.2 shows the amount of wheel slip for different surfaces when the vehicle brakes with a linearly increasing braking torque. The torque has been normalized to improve readability. The maximum torque is speculative, approximated from [14] where typical maximum torque values was 2000 Nm per wheel for a car with a weight of 2000 kg. The assumption is that the brake torque scales linearly with the weight of the vehicle. The wheel loader data used in the simulation had a weight of 8000 kg, which is four times greater hence the maximum torque, $T_{b,max}$, was approximated to 8000 Nm per wheel. One important thing to note from the results in Figure 6.2 is that wheel-lock only occurred on snow.

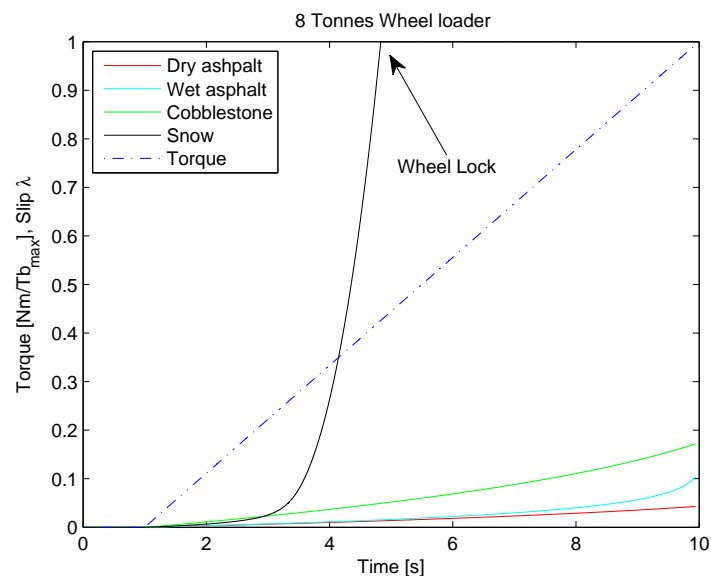


Figure 6.2. Amount of slip for different surfaces for a typical modern medium sized wheel loader

6.1.3 Retardation Controller

The retardation controller was tested with a reference step of $a_{ref} = -1 \text{ m/s}^2$ applied at time $t = 1 \text{ s}$. The result from the reference step test is shown in Figure 6.3. From this plot the closed-loop system's time constant can be computed as $\tau = 86 \text{ ms}$, one can also notice that the system has no overshoot.

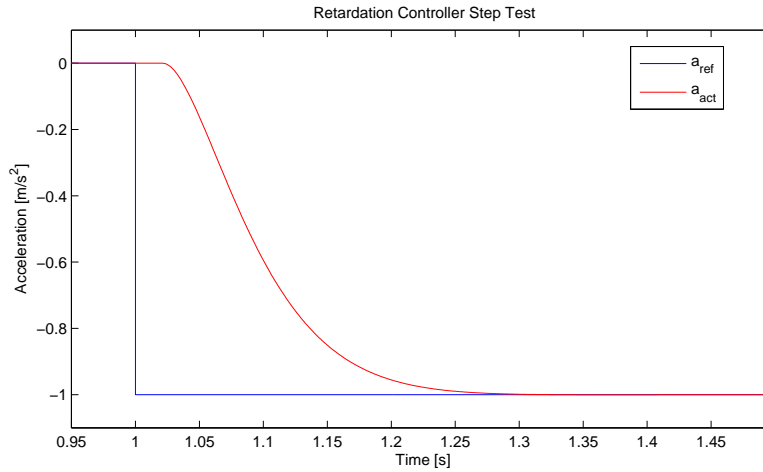


Figure 6.3. Retardation controller step test

6.1.4 Anti-lock system

The anti-lock system was simulated with an initial vehicle velocity of 35 m/s traveling on snow. The torque was requested as a triangular pulse wave in order to capture the activation and deactivation of the slip controller. The torque request is illustrated in Figure 6.4.

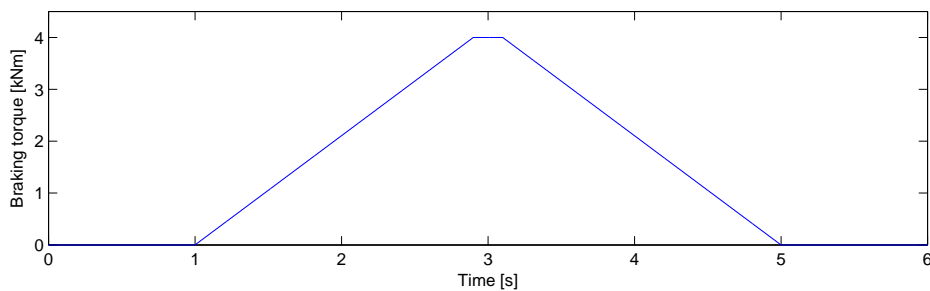


Figure 6.4. Torque request fed to the anti-lock system

The behavior of the wheel slip is presented in Figure 6.5. The anti-lock controller is activated when the slip exceeds the slip threshold². The controller keeps the wheel

²The full activation criteria and switching logic is described in Chapter 4.4

slip around the setpoint until the system is deactivated. The controller has a bit of overshoot, more than anticipated from the controller design, however this is not critical and the system is stable.

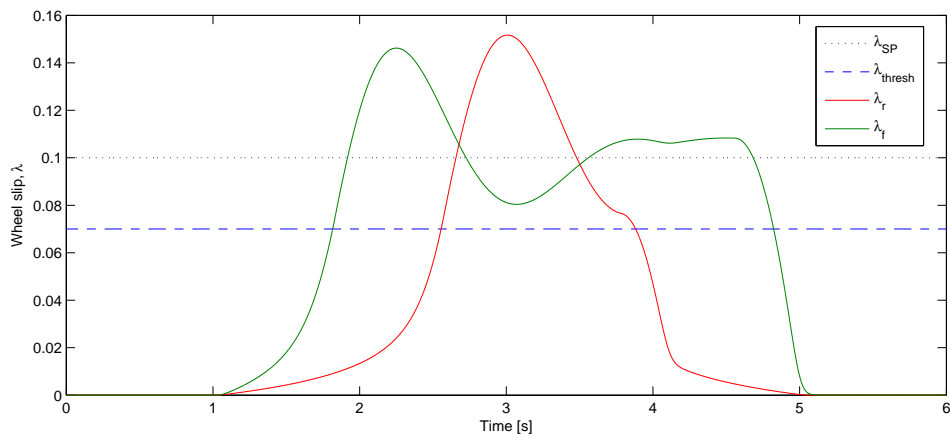


Figure 6.5. Wheel slip

Figure 6.6 illustrates how the output torque is limited by the anti-lock system. The blue line is the requested amount of torque on the wheels but is limited by the anti-lock controller. The green and red line is the brake torque on the front and rear wheels, respectively.

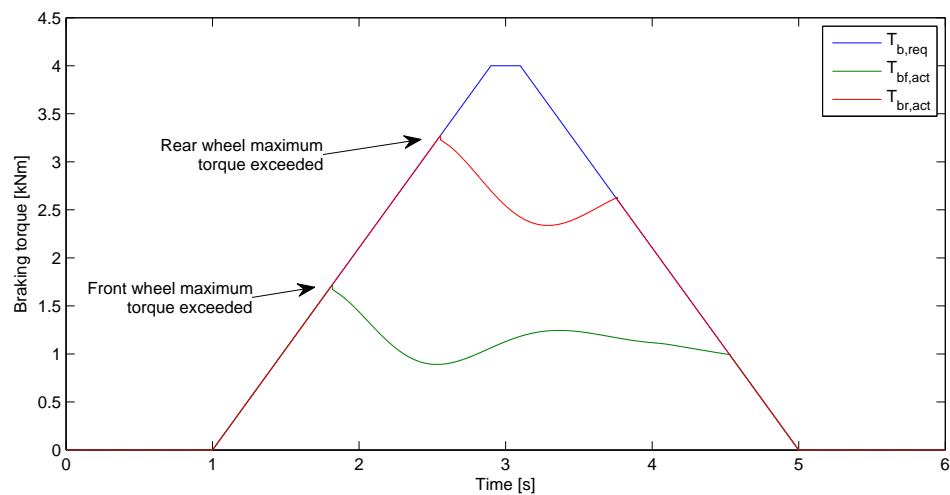


Figure 6.6. Torque requested and torque output

6.1.5 State Observer

The state observer was tested by applying a non-constant torque to both the front and rear wheel. The initial vehicle velocity was set to 40 m/s to allow for a longer braking time. The signals fed to the observer are the wheel velocity of the two wheels, ω_f and ω_r , and the acceleration a , zero mean Gaussian noise was added to the three signals. The actual and the estimated vehicle responses are presented in Figure 6.7. The root mean square (RMS)³ errors are presented in Table 6.2.

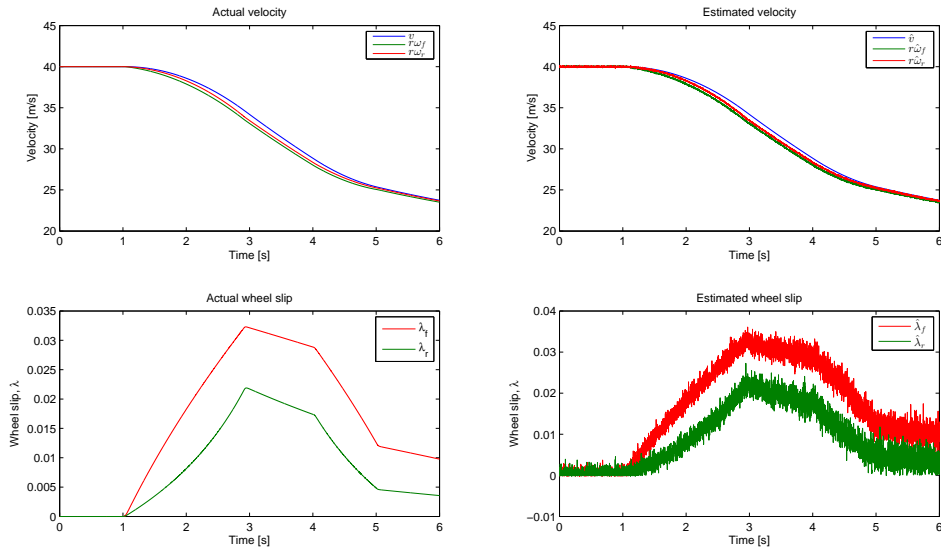


Figure 6.7. State actual values (left) and state estimated values (right)

Table 6.2. RMS error for different states

Variable	RMS error
λ_f	0.004154
λ_r	0.004969
ω_f	0.023718
ω_r	0.041913
v	0.051674

The errors are small however the magnitude is very dependent on the assumptions made on the noise which was speculative at the time the test were conducted.

³computed as $e_{RMS} = \sqrt{\frac{1}{T} \sum_0^T (y - \hat{y})^2}$

6.2 Bench Testing

Modular testing of the subsystems was conducted before implemented in a vehicle. Hardware available at this point are an ECU, a brake actuator, an IMU and a brake pedal.⁴ A personal computer acted as the Driveline Control to send messages over CAN.

6.2.1 Actuator Controller

The actuator controller was tested using a pulse train reference with amplitude 0.3 A, see Figure 6.8. The reference amplitude is approximately half of the valve's maximum current and was chosen to allow for controller overshoot and prevent saturation of the control signal.

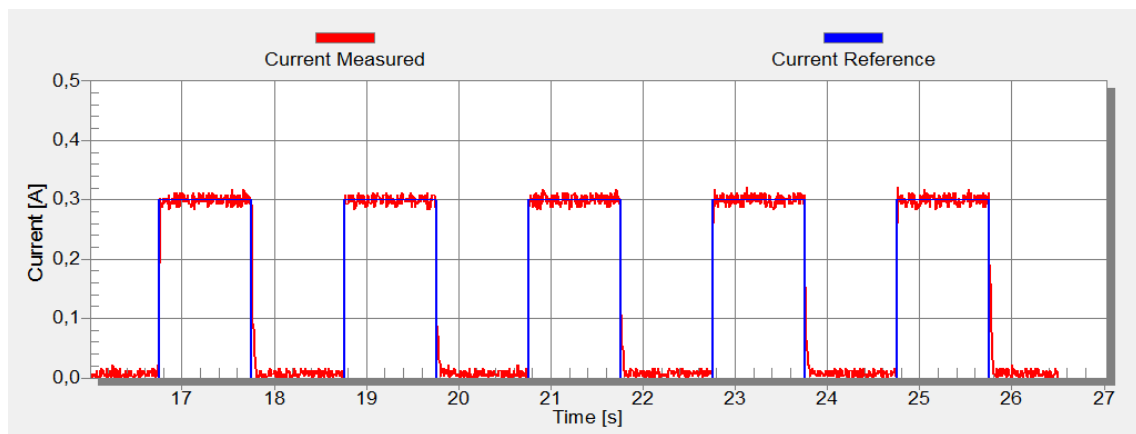


Figure 6.8. Current controller repeated step test

A close-up on one of the reference steps is shown in Figure 6.9. From this dataset the closed-loop system's time constant τ can be approximated to $\tau \approx 2$ ms, the dead time is approximately zero.

6.2.2 Brake Pedal Controller

The brake pedal controller is essentially an open-loop mapping from brake pedal actuation to current driving the actuator. Figure 6.10 shows how the measured current follows the current setpoint given by the brake pedal, when the brake pedal is randomly actuated.

⁴Further described in Chapter 2.1.

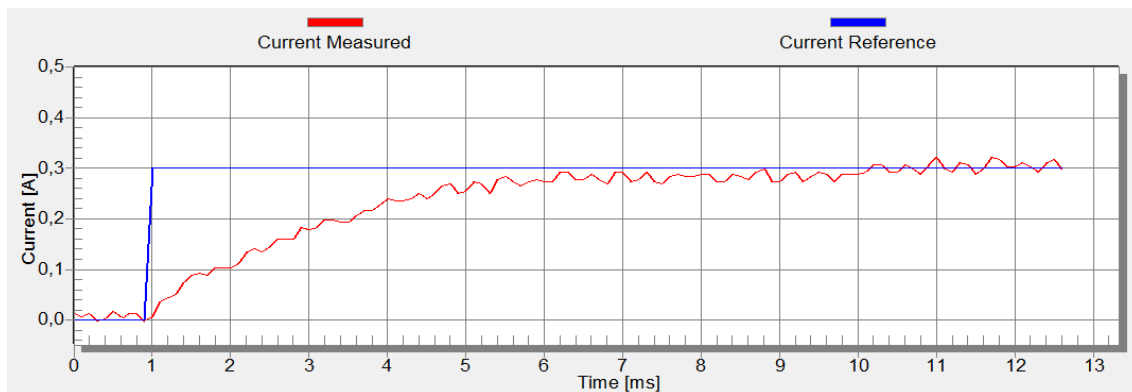


Figure 6.9. Current controller step test

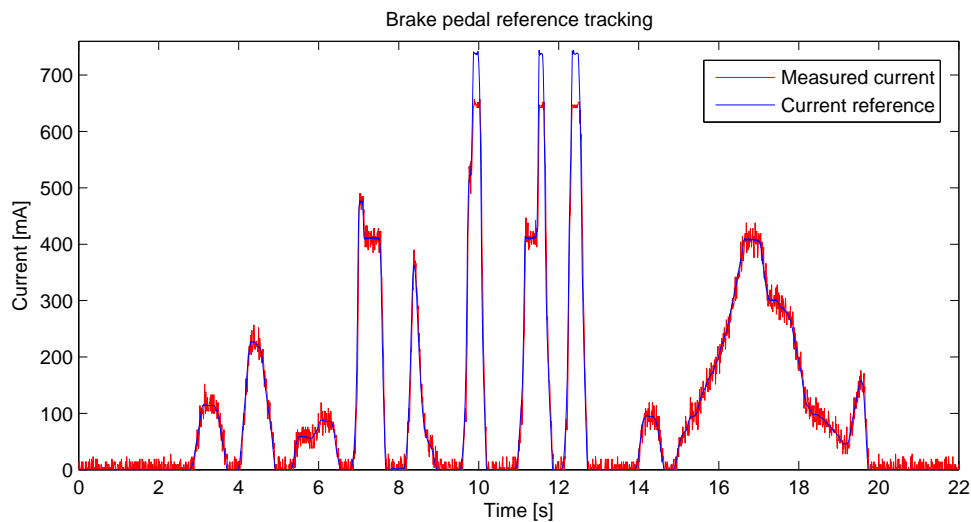


Figure 6.10. Current measurement and current reference set by the brake pedal.

6.2.3 Retardation Controller

The retardation controller is hard to verify in a bench test due to the fact that there is no physical coupling between current output and measured acceleration. Figure 6.11 shows how the measured current follows the current setpoint given by the retardation controller when trying to follow a 0 m/s^2 acceleration reference when the IMU is randomly moved.

6.2.4 Entire System

The bumpless transfer between the brake controller and retardation controller was tested by sending a fix acceleration reference to the retardation controller and giving random inputs with the brake pedal. Figure 6.12 shows how the retardation controller is controlling the output when the driver suddenly presses the brake pedal.

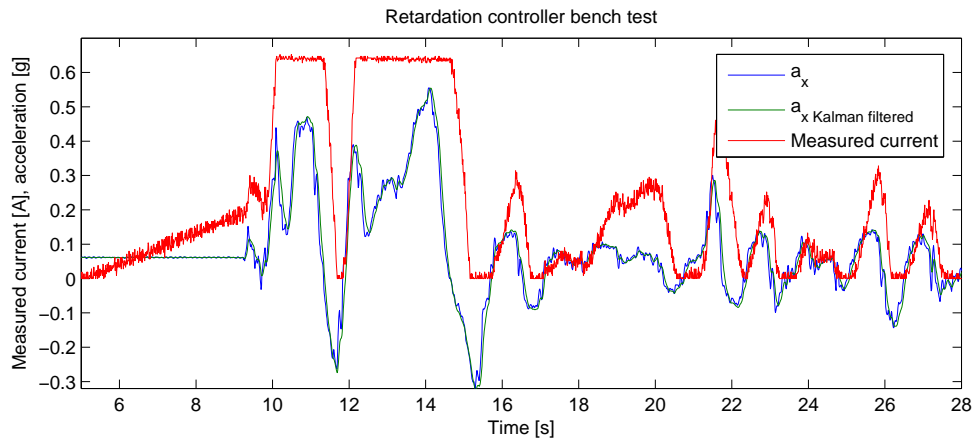


Figure 6.11. Current measurement and current reference set by the retardation controller.

The controller selector always gives priority to the brake pedal, the retardation controller is allowed to execute at every time instance where the brake pedal is not active, i.e. zero input. The transitions between the controllers are smooth and with no integral wind-up. However, switching from the retardation controller to the brake pedal controller results in a rapid drop in control output, shown at time $t \approx 9$ s in Figure 6.12. This behavior is desirable since the driver should have full control over the vehicle. One important note is that the measured acceleration and the retardation controller are physically decoupled in this test, i.e. dynamic properties can not be identified from the graph.

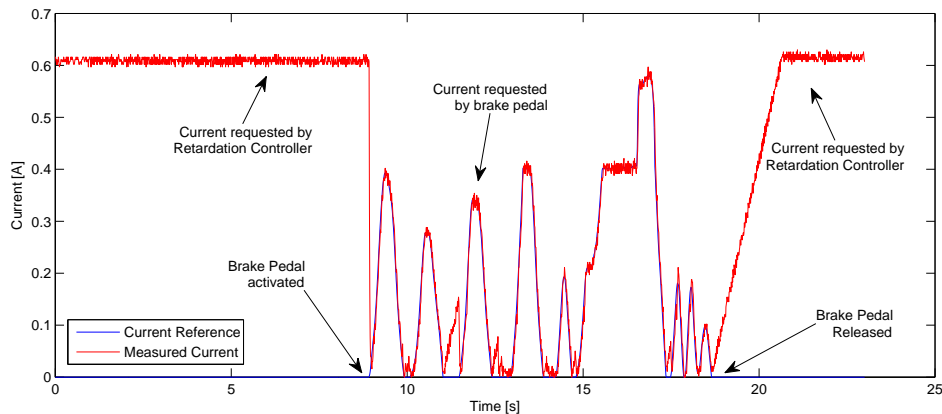


Figure 6.12. Bumpless switching between the brake pedal and the retardation controller

6.3 Vehicle Testing

The test vehicle was a Volvo L220F wheel loader, this machine has dual brake circuits on the front axis and a single brake circuit on the rear axis. This brake system was attached to one of the circuits, the other connected to the vehicle's brake pedal to allow for emergency braking. In each of the tests the vehicle speed was ~ 8 m/s driving back and forth on a flat horizontal pavement surface. The actuator had a offset of 270 mA, the controllers were redesigned so that when active, the initial output current would jump to this value to prevent unnecessary current drain.

Due to time restrictions, only three different tests were conducted:

1. Current step test.
2. Acceleration step test
3. Brake pedal functionality test

Since the state estimator was not used during vehicle test because of time restrictions, which is further discussed in Chapter 7, a simple Kalman filter was created to post process the accelerometer data. The Kalman filter is based on *jerk* which means that the model is based on the time derivative of the acceleration. This filter is presented in Appendix C.

6.3.1 Current Step Test

Three different step sizes was used in order to minimize and highlight the effect of possible nonlinearities. The intention with the step tests is to extract the dynamics of the system. From a step test it is possible to identify the dynamic properties such as the systems time constant and dead time. Figure 6.13 shows a 560 mA step test, graphs from the other two step test are found in Appendix D. The estimated dynamic properties are presented in Table 6.3. The oscillations occurring after vehicle standstill, pointed out in the plots, are due to the vehicle wiggling back and forth.

Table 6.3. Approximated dynamic properties for the different current step tests

Reference step	Time Constant Solenoid	Actuator Delay	Time Constant Vehicle
440 mA	20 ms	330 ms	320 ms
560 mA	30 ms	330 ms	250 ms
660 mA	35 ms	330 ms	130 ms
Average	28 ms	330 ms	230 ms

The results from a 560 mA step test with and without dithering is presented in Figure 6.13 and Figure 6.14, respectively.

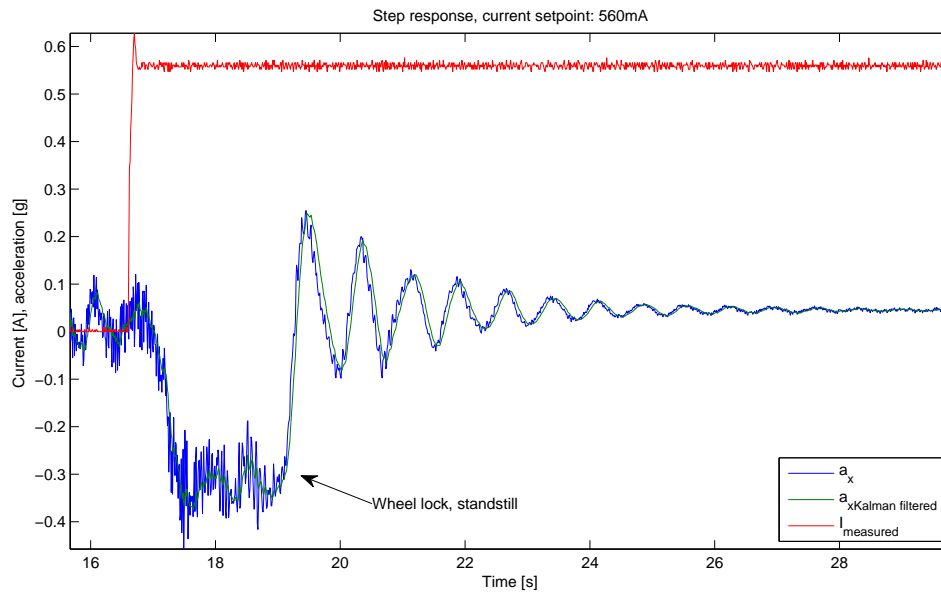


Figure 6.13. 560 mA step test, dithering disabled

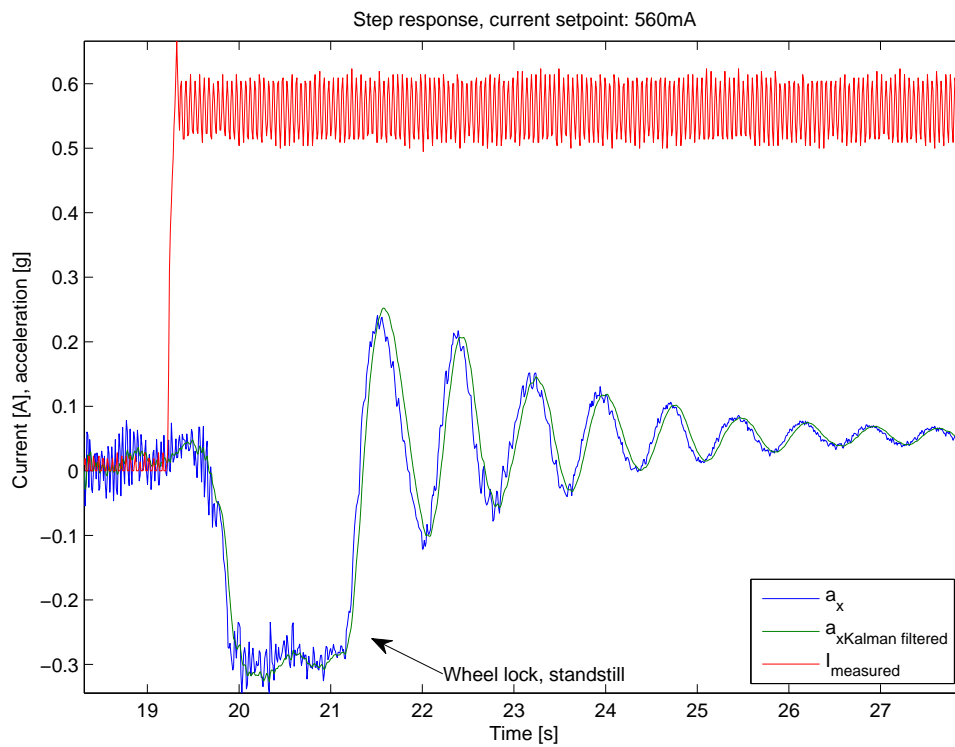


Figure 6.14. 560 mA step test, dithering enabled

Table 6.4. Approximated dynamic properties for a 560 mA step with and without dithering

	Time Constant Solenoid	Actuator Delay	Time Constant Vehicle
Dither Off	30 ms	330 ms	250 ms
Dither On	35 ms	330 ms	260 ms

6.3.2 Acceleration Step Test

An acceleration step test was conducted to verify the retardation controller's functionality. Three different retardation requests was sent to the controller. In the first test the controller parameters were the same as those derived from the mathematical models, the result is shown in Figure 6.15. As can be seen from the plot the controller is unstable with an oscillating behavior.

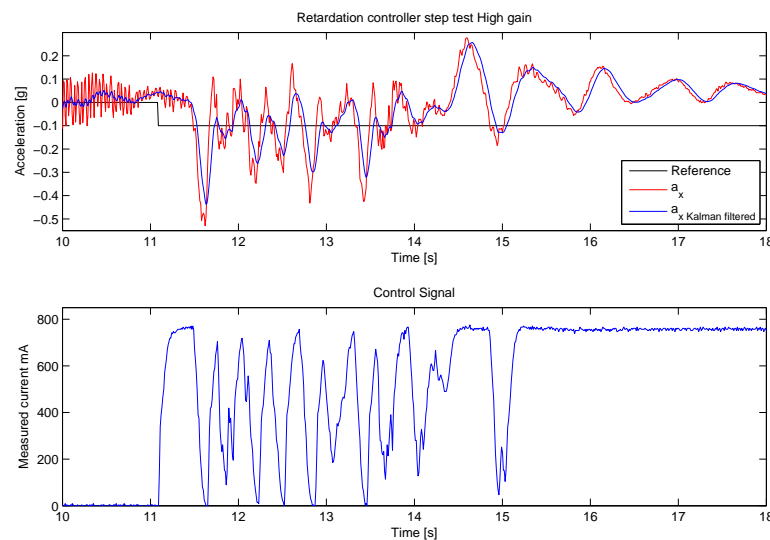


Figure 6.15. Retardation controller step test, high gain

Further step tests were conducted with a lower gain of the controller parameters. Figure 6.16 shows the step response with a significantly lower controller gain compared to the first controller.

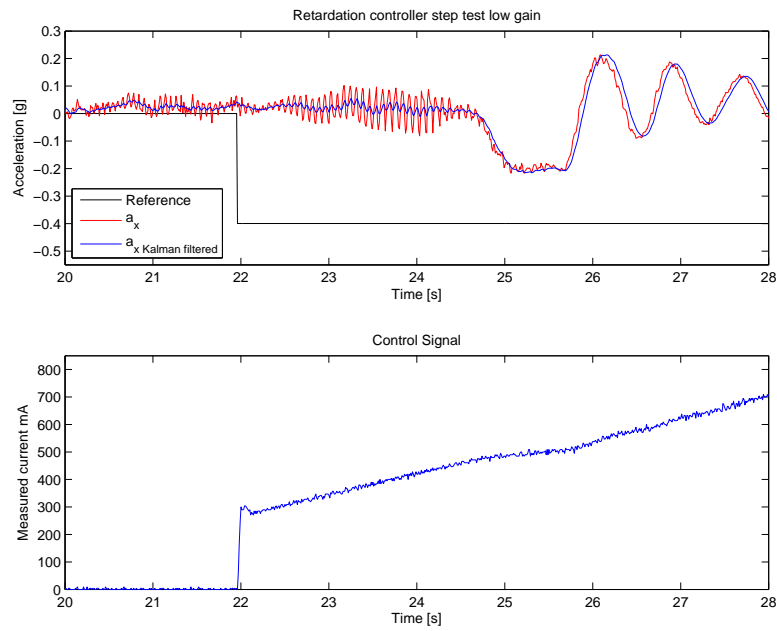


Figure 6.16. Retardation controller step test, low gain

Figure 6.17 shows the step response with a somewhat higher controller gain than in Figure 6.16. Both controllers are stable but very slow.

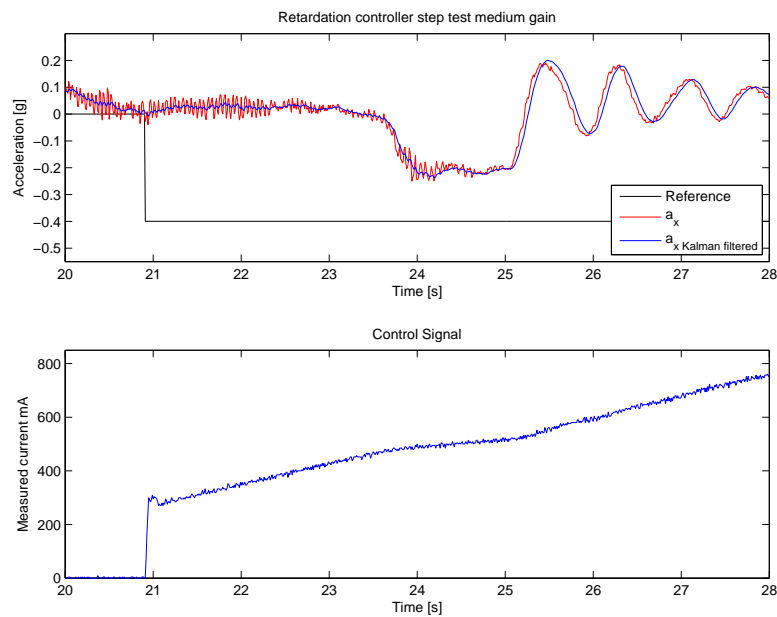


Figure 6.17. Retardation controller step test, medium gain

6.3.3 Brake Pedal Functionality Test

The brake pedal functionality is the most difficult part to verify. The requirement on the system is that it should have more or less the same performance as the normal brake pedal system. Two different mappings were tested, these two mappings are presented in Figure 6.18. One has a linear increase of torque request and one has a progressive increase. According to the test driver the linear mapping felt more intuitive and mimicked the behavior of the traditional brake pedal better. A brake test with the brake pedal and the linear mapping is presented in Figure 6.19.

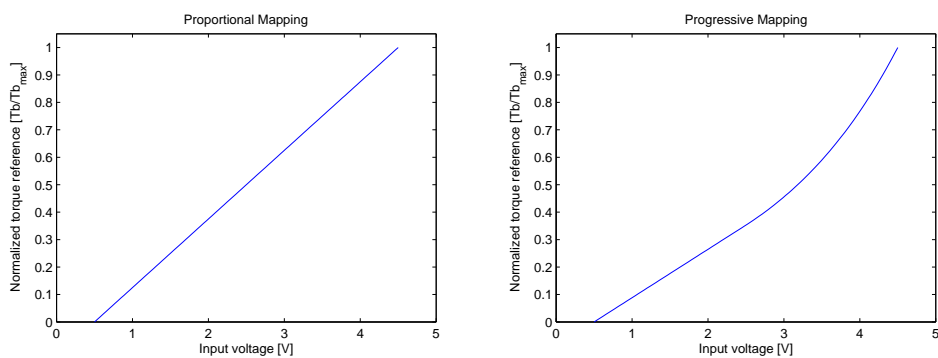


Figure 6.18. Brake pedal controller input-output mapping, *left*: linear mapping, *right*: progressive mapping

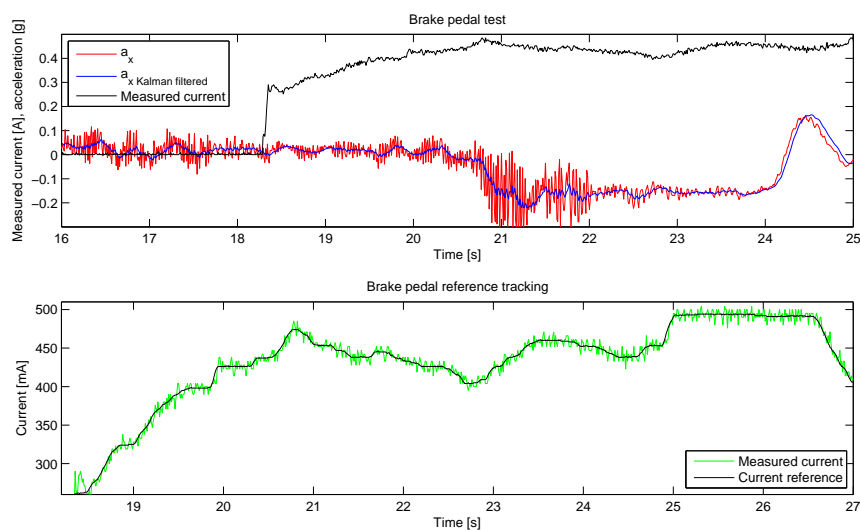


Figure 6.19. Brake pedal test on vehicle

6.4 Risk Analysis and Safety Assessment

A risk analysis and safety assessment was conducted according to Chapter 5. The result is presented in this chapter.

6.4.1 Item Definition

The item was defined according to Figure 6.20, the subparts of the item are further described in Chapter 2.2. The hazard analysis was conducted at the vehicle level¹.

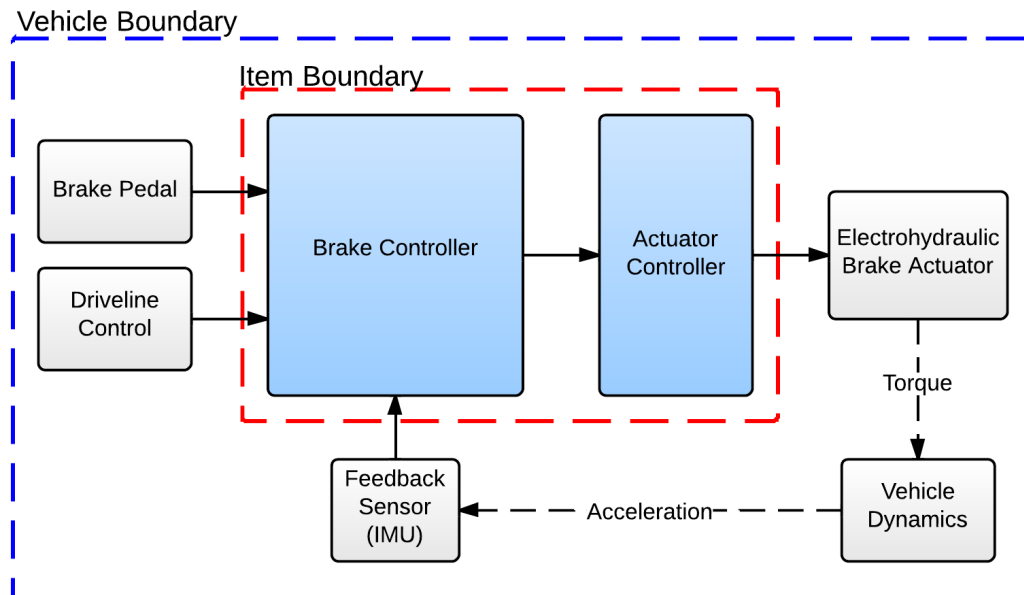


Figure 6.20. Item definition

6.4.2 Operational Situations

In order to identify the hazardous events, the vehicle's operational scenarios and conditions has to be specified. Three machine operational situations were identified together with five different surface properties, presented in Table 6.5 and Table 6.6, respectively. This rendered a total of 13 operational situations presented in Table A.1. With these operational situations, the analysis is continued with the help of the tables presented in 5. Each operational situation is then defined in terms of; *Controllability*, *Exposure* and *Severity* which gives a ASIL grade.

¹Marked as *Vehicle Boundary* in Figure 6.20

Table 6.5. Operational situations

Machine operation		Details
Loading or unloading	Short cycle operation	At standstill, parking brake not engaged
Low speed	Max speed according to operators manual, chute/bucket can be loaded or empty	Speed < 25 km/h
High speed	Travelling at public or private (construction site) roads, at max. speed (empty chute/bucket)	25 – 60 km/h

Table 6.6. Surface properties

Surface properties	Description	Details
Flat	Flat surface, good traction.	
Inclination	Machine traveling up- or downhill, good traction	Inclination considered is 10°
Slippery	Flat surface, snow or wet mud, traction is poor.	
Slippery inclination	Machine traveling up- or downhill in slippery conditions, traction is poor	Inclination considered is 10°
Public road	Machine traveling at public road, various conditions.	Other vehicles and VRUs present

6.4.3 System Malfunctions

All of the operational situations that gave a higher grade than *quality management*(QM) could be simplified and three possible system malfunctions at the vehicle level were identified, these are presented in Table 6.7.

Table 6.7. System malfunctions

ID	Malfunction	Failure mode description
MF1	Loss of braking power	Brake system does not respond to brake requests
MF2	Unintended braking	Any braking done by the system without a present brake request
MF3	Erratic braking	The system responds to the brake requests, but not in a predictable way.

6.4.4 Hazard analysis and Risk Assessment

The result from the hazard analysis⁵ rendered the safety goals described in Table 6.8.

Table 6.8. Safety Goals

ID	Safety Goal	Highest ASIL
SG1	No loss of braking power	ASIL D
SG2	No unintended braking	ASIL B
SG3	No erratic braking	ASIL C

6.4.5 Functional Safety Concept

The functional safety requirements were derived through fault tree analysis (FTA) of how item malfunctions will violate the safety goals. The FTA on each of the safety goal are presented in Figure B.1, Figure B.2 and Figure B.3 in Appendix B. The corresponding functional safety requirements are found in Table 6.9.

Table 6.9. Functional Safety Requirements

ID	Description	Safety goal	Highest ASIL	Fault Detection
FSR_1	No faulty signal from Driveline Control	SG1, SG2, SG3	ASIL D	Allocate on Driveline Control supplier
FSR_2	No faulty signal from IMU	SG1, SG2, SG3	ASIL D	Allocate on IMU supplier
FSR_3	No faulty signal from brake pedal	SG1, SG2, SG3	ASIL D	Dual, independent signals from brake pedal
FSR_4	No Faulty Torque Request Output from Brake Controller	SG1, SG2, SG3	ASIL D	Dual independent controllers will compute the same output
FSR_5	No Faulty Actuation Signal from Actuator Controller	SG1, SG2, SG3	ASIL D	Actuation signal shall be monitored by external independent process

⁵Unfortunately unavailable due to confidentiality reasons.

7 Discussion

7.1 Brake Pedal Controller

It was difficult to verify the brake pedal's performance since it was hard to define and mimic the feel of the original brake pedal. Since we, the authors, did not drive the vehicle it was hard to interpret how the driver felt when he used the brake pedal. The test driver mentioned that it usually takes a lot of time and testing to get the feeling right, and it is almost essential that the one evaluating the brake pedal is the one designing the brake mapping.

7.2 Retardation controller

The retardation controller's performance were nowhere near as good as in the simulations. The test of the first controller, with parameters derived from the mathematical model, resulted in a unstable system. The controller did not manage to track the reference, as seen in Figure 6.15. From the step test results it is clear that the real system and the mathematical model are very different. In the simulations the dead time of the system was approximated to 20 ms, which was based on an assumption given by [15]. The actual dead time was approximately 330 ms. This great difference in dead time is probably why the system got unstable since longer dead time heavily increases the phase lag which decreases the stability margins.

An other issue that arose was that the controller would give maximum braking torque when the vehicle was very close to standstill. This would yield a very harsh stopping bump and the vehicle would rock back and forth, as can be seen in Figure 6.13. This could be prevented by adding a outer loop controlling the vehicle velocity which could give a much smoother transition to standstill.

7.3 Dithering

Dithering was expected to have a greater impact on the system's performance. No difference in the step response with respect to dead time could be noted. This could be due to that the current generated by the step is sufficiently large to move the plunger, instantaneous within the time scale, such that the stiction is negligible. The only difference between the two step tests is that the acceleration is somewhat smoother with dithering, which could mean that dithering has a positive impact on the brake pressure, but could also be due to the fact that the vehicle happens to be driving on a somewhat smoother part of the test area. Figure 7.1 illustrates the difference between the case when dithering was enabled and disabled. Unfortunately

no dither test were conducted on the retardation controller or with the brake pedal where the dithering would presumably have had a greater impact because of the smaller increments in the current.

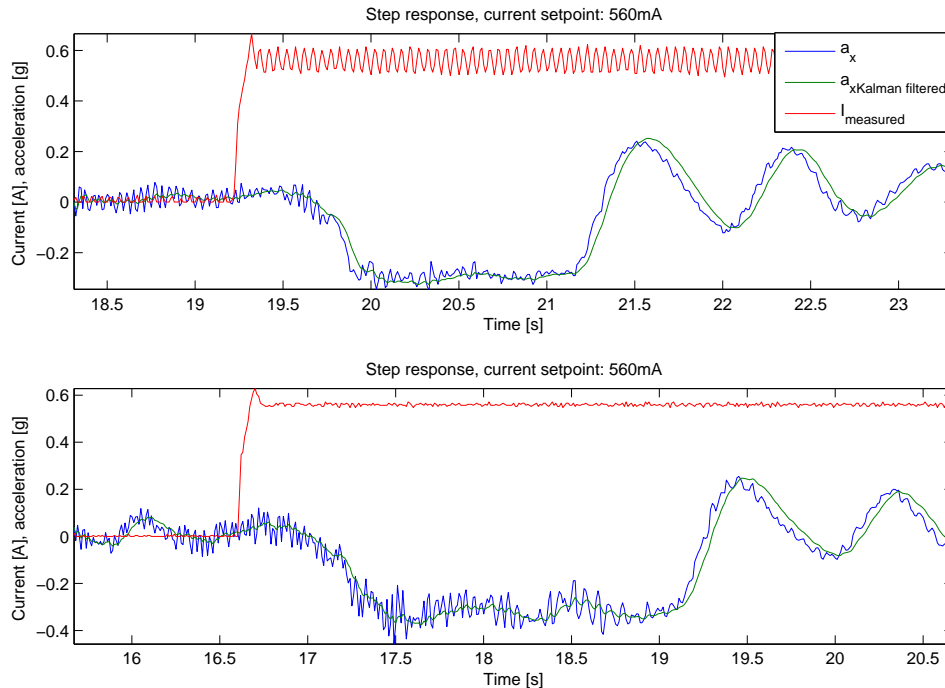


Figure 7.1. Comparison between step tests, with and without dithering

7.4 State estimator and Slip controller

The simulations show that the state estimator and the wheel slip controller design is feasible. The slip controller has a rather large overshoot for being designed as a well damped system. This could be due to the fact that the system is designed for the single corner model but simulated on the enhanced dual corner model. The RMS error of the estimated parameters shows promising results in future implementation of the algorithm, however the error is highly dependent of the variance of the added Gaussian noise which could have been wrongly approximated.

The state estimator and the slip controller was not implemented nor tested on the actual system, this was mainly due to the fact that the test vehicle lacked the possibility to measure the velocity on each wheel independently and also lacked the possibility to control the braking torque on each wheel independently. Furthermore, the time available to test the system was very limited and focus lay on verifying the primary control system, i.e the actuator controller, brake pedal controller and retardation controller.

7.5 Future Work

The retardation controller should be revised since it was clear that the dynamics in the model differed too much from the real system. Though tuning with the implemented controller on real test could be adequate.

The brake pedal needs further testing in order to achieve a brake pedal that could replace the original one in terms of feel.

In order to assure the safety integrity for commercial use of the system the ISO-26262 analysis should be continued.

8 Conclusions

The scope of this thesis is to develop a so called brake-by-wire system for construction vehicles. The system should be able to handle both normal brake pedal functionality and closed-loop retardation control.

The mathematical models that covers brake torque to vehicle acceleration has been shown to be insufficient. It has been concluded that the main reasons for this is the assumptions made on the dynamics from the solenoid actuator to the actual brake torque on the wheels capture the real behavior poorly.

8.1 Brake system

From the live test it has been shown that the fundamental parts of the brake system is functional. The brake pedal was reliable and had a good performance in terms of response time and accuracy, though more testing needs to be done to mimic the behavior of the traditional brake pedal. The current controller managed to keep the desired current and had a good response time. The retardation controller did however not function according to specification or theoretical data from simulations. To improve the performance, the model has to be revised with the vehicle dynamics data acquired from the live test. Also to achieve a fully functional retardation controller the controller should be extended with an additional controller in order to identify whether the vehicle is near standstill or not. This problem could also be solved externally by the driveline control.

The slip dynamics and properties obtained from the mathematical models could not be verified on the test vehicle. From simulation results it has been shown that a locking situation with unstable braking is only probable on poor surface conditions, i.e snow/ice or similar. With these results the motivation of adding an anti-lock system is not cogent, a survey with drivers attending the severity and probability of wheel lock could be carried out to obtain a final conclusion.

8.2 Safety assessment

From the safety assessment according to ISO-26262 it has been concluded that the brake system is a safety critical system. The functional safety concept rendered an ASIL D classification on all functional safety requirements.

Bibliography

- [1] V. Askue. Fly-by-wire. *Air Medical Journal*, 22(6):4–5, 2003.
- [2] R.P.G. Collinson. *Introduction to Avionics Systems*. Springer, third edition, 2011.
- [3] L.F.E. Coombs. The aircraft cockpit: from stick-and-string to fly-by-wire. *Applied Ergonomics*, 23(4), 1992.
- [4] R.E. Kalman. A new approach to linear filtering and prediction problems. *Basic Engineering*, 82, 1960.
- [5] B. Lennartson. *Reglerteknikens grunder*. Studentlitteratur, 2000.
- [6] N.A. Stanton; P. Marsden. From fly-by-wire to drive-by-wire: Safety implications of automation in vehicles. *Safety Science*, 24(1):35–49, 1996.
- [7] International Standard Organisation. *ISO 26262 - Road vehicles - Functional safety*.
- [8] P. Gradin; V. Ortman. Development of a collision avoidance truck system from a functional safety perspective.
- [9] H.B. Pacejka. *Tire and Vehicle Dynamics*. Elsevier, third edition, 2012.
- [10] Mpu 6000 and mpu 6050 product specification.
- [11] F. Randy. X-by-wire: For power, x marks the spot. *Ward's Auto World*, 40(10):26–30, 2004.
- [12] K.J. Åström; R.M. Murray. *Feedback Systems*. Princeton University Press, 2008.
- [13] K.J. Åström; T. Hägglund. Revisiting the ziegler-nichols step response method for pid control. *Journal of Process Control*, 2004.
- [14] K.B. Singh; M.A. Arat; S. Taheri. An intelligent tire based tire-road friction estimation technique and adaptive wheel slip controller for antilock brake system. *Journal of Dynamic Systems, Measurement, and Control*, 135(3), 2013.
- [15] S.M. Savaresi; M. Tanelli. *Active Braking Control Systems Design for Vehicles*. Advances in Industrial Control. Springer, London, 1st edition, 2001.

A Operational Situations and Corresponding Exposure

Table A.1. Operational situations identified and their rate of exposure

	Operational Situation	Exposure	
OP1	Loading or unloading on flat surface	High exposure, conducted several times every work shift	E4
OP2	Loading or unloading on inclination	Not very probable. Most unloading operations will be performed on flat surface	E2
OP3	Loading or unloading on flat slippery surface	Low to medium exposure. Most loading and unloading operations are considered to be conducted on appropriate surface	E2
OP4	Loading or unloading on slippery inclination	Low exposure, loading or unloading will most unlikely be performed on slippery inclination	E1
OP5	Traveling at low speed on flat surface	High exposure, conducted several times every work shift	E4
OP6	Traveling at low speed on inclination	High exposure, conducted several times every work shift	E4
OP7	Traveling at low speed on slippery surface	Medium exposure	E3
OP8	Traveling at low speed on slippery inclination	Low exposure, not the most common surface combination	E2
OP9	Traveling at high speed on flat surface at worksite	High exposure, conducted several times every work shift	E4
OP10	Traveling at high speed on inclination at worksite	High exposure, conducted several times every work shift	E4
OP11	Traveling at high speed on slippery surface at worksite	Not very probable, operator will most likely adopt the speed to current surface conditions	E1
OP12	Traveling at high speed on slippery inclination at worksite	Unlikely, operator will most likely adopt the speed to current surface conditions	E1
OP13	Traveling at high speed on public road	Unlikely, public roads are mostly used for transportation of machine between worksites	E1

B Fault Tree Analysis

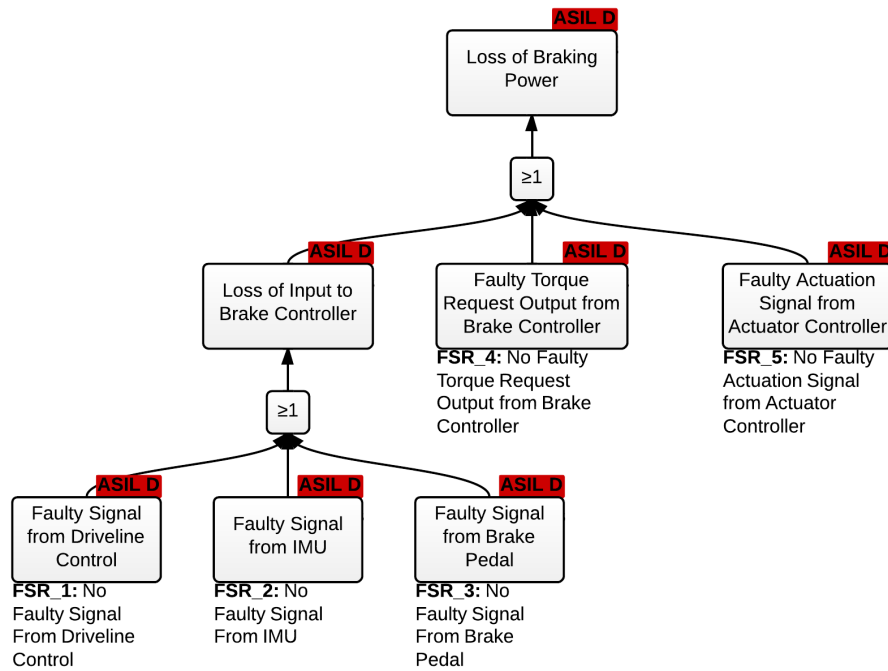


Figure B.1. FTA on safety goal 1 violation

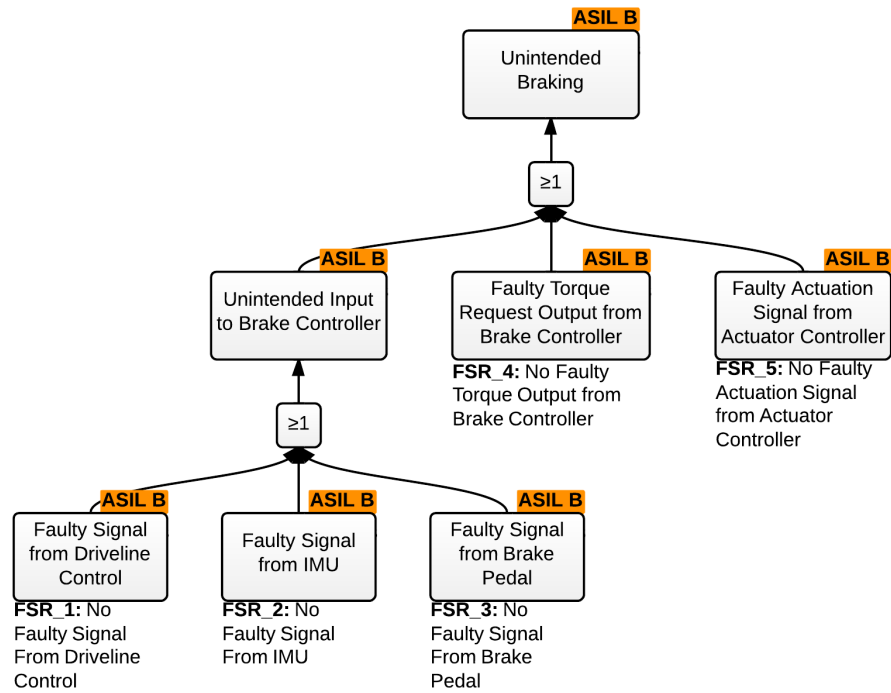


Figure B.2. FTA on safety goal 2 violation

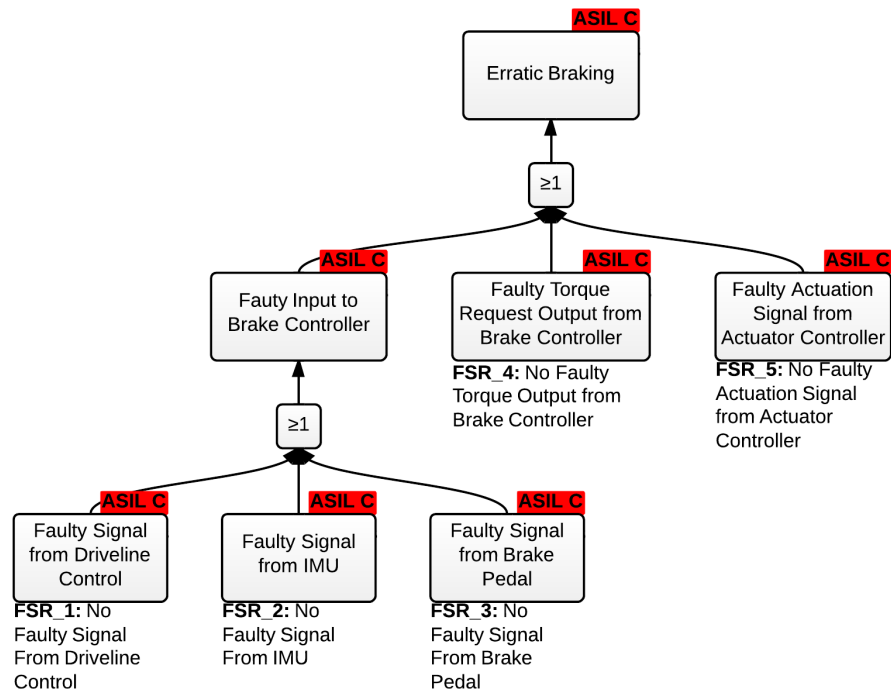


Figure B.3. FTA on safety goal 3 violation

C Kalman Filter Based on Jerk

The discretized model of acceleration, using the Forward Euler method, can be described as

$$a_k = a_{k-1} + \Delta t \cdot \dot{a}_{k-1} \quad (\text{C.1})$$

This system can be rewritten on state space form, the states are chosen as $x = \begin{bmatrix} a \\ \dot{a} \end{bmatrix}$ which would give

$$x_k = \begin{bmatrix} 1 & \Delta t \\ 0 & 1 \end{bmatrix} x_{k-1} \quad (\text{C.2})$$

This system can be estimated by a Kalman filter. The filter uses a predict and update algorithm according to

Predict

$$\begin{aligned} \hat{x}_{k|k-1} &= F \hat{x}_{k-1|k-1} \\ P_{k|k-1} &= F P_{k-1|k-1} F^T + Q \end{aligned}$$

Update

$$\begin{aligned} \tilde{y}_k &= z_k - H_k \hat{x}_{k|k-1} \\ S_k &= H_k P_{k|k-1} H_k^T + R_k \\ K_k &= P_{k|k-1} H_k^T S_k^{-1} \\ \hat{x}_{k|k} &= \hat{x}_{k|k-1} + K_k \tilde{y}_k \\ P_{k|k} &= (I - K_k H_k) P_{k|k-1} \end{aligned}$$

where Q is the process noise, R is the measurements noise, $H = [1 \ 0]$ is the output select matrix, $F = \begin{bmatrix} 1 & \Delta t \\ 0 & 1 \end{bmatrix}$, z_k is the acceleration measurement, P is the covariance estimate matrix, \tilde{y} is the measurement residual, S is the residual covariance and K is the near optimal Kalman gain.

D Current Step Test of Real Vehicle

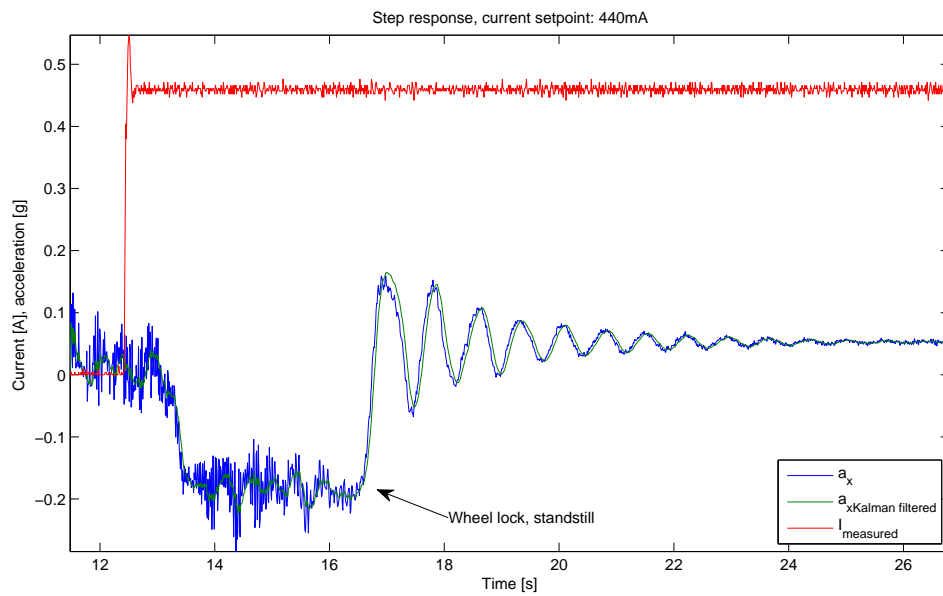


Figure D.1. 460 mA step test, dithering disabled

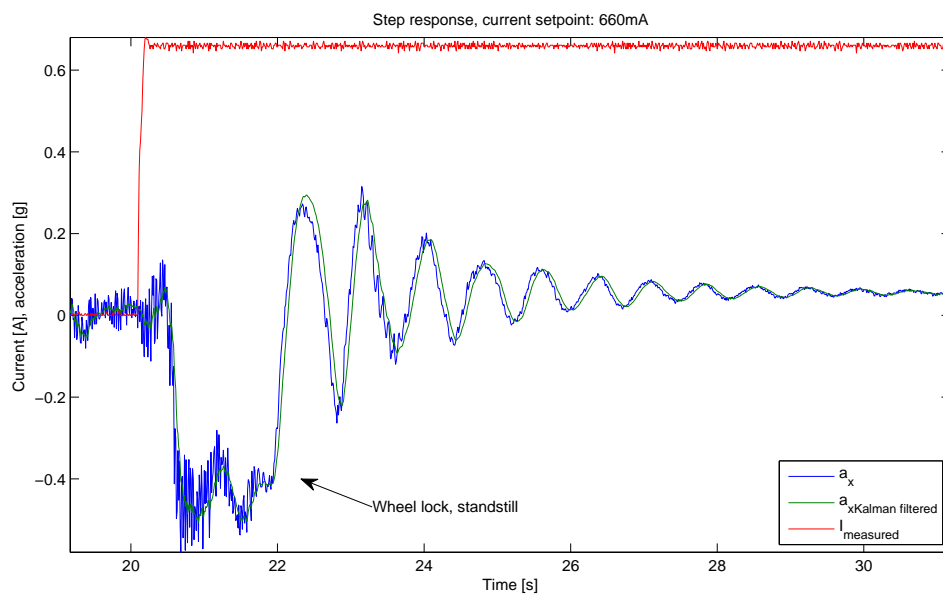


Figure D.2. 660 mA step test, dithering disabled